

N₂O isotope approaches for source partitioning of N₂O production and estimation of N₂O reduction – validation with ¹⁵N gas-flux method in laboratory and field studies

Dominika Lewicka-Szczebak^{1,2}, Maciej Piotr Lewicki³ and Reinhard Well⁴

5 ¹ Centre for Stable Isotope Research and Analysis, University of Göttingen, Büsgenweg 2, 37077 Göttingen, Germany

² Institute of Geological Sciences, University of Wrocław, pl. M. Borna 9, 50-204 Wrocław, Poland

³ Institute of Theoretical Physics, University of Wrocław, pl. M. Borna 9, 50-204 Wrocław, Poland

⁴ Thünen-Institut of Climate-Smart Agriculture, Bundesallee 50, 38116 Braunschweig, Germany

10 *Correspondence to:* Dominika Lewicka-Szczebak (dominika.lewicka-szczebak@uwr.edu.pl)

Abstract.

The approaches based on natural abundance N₂O stable isotopes are often applied for the estimation of mixing proportions between various N₂O producing pathways as well as for estimation of the extent of N₂O reduction to N₂. But such applications are associated with numerous uncertainties and hence their limited accuracy needs to be considered. Here we present the first systematic validation of these methods for laboratory and field studies applying the ¹⁵N gas-flux method as the reference approach.

Besides applying dual isotope plots for interpretation of N₂O isotopic data, for the first time we propose a three dimensional N₂O isotopocule model based on Bayesian statistics to estimate the N₂O mixing proportions and reduction extent based simultaneously on three N₂O isotopic signatures ($\delta^{15}\text{N}$, $\delta^{15}\text{N}^{\text{SP}}$ and $\delta^{18}\text{O}$). Determination of mixing proportions of individual pathways with N₂O isotopic approaches appears often imprecise, mainly due to imperfect isotopic separation of the particular pathways. Nevertheless, the estimation of N₂O reduction is much more robust, when applying optimal calculation strategy, reaching typically accuracy of N₂O residual fraction determination of about 0.15.

25 1. Introduction

Nitrous oxide (N_2O) emission from soils and waters may result from numerous nitrogen transformation processes, mainly heterotrophic bacterial denitrification (bD), autotrophic nitrification (Ni), nitrifier denitrification (nD), and fungal denitrification (fD), but also heterotrophic nitrification, chemodenitrification, or co-denitrification (Butterbach-Bahl et al., 2013; Firestone and Davidson, 1989; Müller et al., 2014). The ability to distinguish the proportional contributions of these various N_2O origins (f_{bD} , f_{Ni} , f_{nD} , f_{fD}) is important for constraining the N budget and for developing and assessing the performance of mitigation strategies for N_2O emission, which significantly contributes to global warming and stratospheric ozone depletion (IPCC, 2007; Ravishankara et al., 2009). Determination of the mixing proportions f_{bD} , f_{Ni} , and f_{nD} is only partially possible by combination of numerous experimental techniques, including sophisticated ^{15}N and ^{18}O isotope labelling techniques (Müller et al., 2014; Wrage-Mönnig et al., 2018). However, also natural abundance N_2O isotopic analyses have been often applied to estimate the possible proportional contribution of particular pathways (Toyoda et al., 2017; Yu et al., 2020) and are currently the only isotopic approach to identify f_{fD} (Rohe et al., 2017; Wrage-Mönnig et al., 2018). The determination of mixing proportions based on natural abundance N_2O isotopes is theoretically possible thanks to characteristic isotopic fractionation for each pathway, determined in numerous laboratory pure culture experiments (Toyoda et al., 2017), but practically very complex, mainly due to changes of N_2O isotopic signature during its partial reduction to N_2 and due to overlapping isotopic endmember values of individual pathways. N_2O isotopic analyses comprise the isotopic determination of: oxygen ($\delta^{18}\text{O}$), bulk nitrogen ($\delta^{15}\text{N}$) and nitrogen site preference ($\delta^{15}\text{N}^{\text{SP}}$), i.e., the difference in $\delta^{15}\text{N}$ between the central and the peripheral N atom of the linear N_2O molecules (Brenninkmeijer and Röckmann, 1999; Toyoda and Yoshida, 1999). All these three isotopic signatures ($\delta^{18}\text{O}$, $\delta^{15}\text{N}$ and $\delta^{15}\text{N}^{\text{SP}}$) show characteristic ranges of isotopic signatures for particular N_2O production pathways but are also altered during the N_2O reduction process.

N_2O reduction to N_2 occurs during the last step of microbial denitrification, i.e., anoxic reduction of nitrate (NO_3^-) to N_2 through the following intermediates: $\text{NO}_3^- \rightarrow \text{NO}_2^- \rightarrow \text{NO} \rightarrow \text{N}_2\text{O} \rightarrow \text{N}_2$ (Firestone and Davidson, 1989; Knowles, 1982). Commonly applied experimental techniques enable us to quantitatively analyse only the intermediate product of this process, N_2O , but not the final product, N_2 (Groffman, 2012; Groffman et al., 2006). This is due to the high atmospheric N_2 background precluding direct measurements of N_2 emissions in presence of the natural atmosphere (Bouwman et al., 2013; Saggarr et al., 2013). Estimation of N_2 -flux is possible with sophisticated laboratory experiments applying N_2 -free helium atmosphere (Scholefield et al., 1997) or ^{15}N gas-flux method, i.e. ^{15}N analyses of gas fluxes after addition of ^{15}N -labelled substrate (Bergsma et al., 2001; Schmidt et al., 1998). Previous studies documented large possible variations in N_2 flux, and consequently also in the residual unreduced N_2O fraction: $r_{\text{N}_2\text{O}} = y_{\text{N}_2\text{O}}/(y_{\text{N}_2} + y_{\text{N}_2\text{O}})$ (y : mole fraction). In laboratory studies, the whole scale of possible $r_{\text{N}_2\text{O}}$ variations, ranging from 0 to 1, had been found (Lewicka-Szczebak et al., 2017; Lewicka-

Szczebak et al., 2015; Mathieu et al., 2006; Morse and Bernhardt, 2013; Senbayram et al., 2012). Due to technical limitations, so far only the ^{15}N gas-flux method had been applied in field conditions to determine $r_{\text{N}_2\text{O}}$ (Aulakh et al., 1991; Baily et al., 2012; Bergsma et al., 2001; Buchen et al., 2016; Decock and Six, 2013; Kulkarni et al., 2013; Mosier et al., 1986). Moreover, first attempt to apply the ^{15}N gas-flux method under N_2 -reduced atmosphere in field has been presented recently (Well et al., 2019a). This new approach increases the sensitivity of ^{15}N gas-flux method (80-fold better sensitivity for $\text{N}_2+\text{N}_2\text{O}$ flux measurements (Well et al., 2019a)) which was so far very limiting for successful application in field studies (Buchen et al., 2016). But still, application of this approach is technically very demanding and applicable only with a low temporal and spatial resolution. Hence, no comprehensive data sets from field-based measurements of soil N_2 emissions are available and this important component in soil nitrogen budget is still missing. This constitutes a serious shortcoming in understanding and mitigating the microbial consumption of nitrogen fertilisers (Bouwman et al., 2013; Seitzinger, 2008), and the N_2O budget.

An alternative approach for assessing N_2 fluxes is the use of N_2O isotopes, which allows to indirectly determine $r_{\text{N}_2\text{O}}$ from the isotopic signature of the residual N_2O (Ostrom et al., 2007; Well and Flessa, 2009), since the increase in $\delta^{18}\text{O}$, $\delta^{15}\text{N}$ and $\delta^{15}\text{N}^{\text{SP}}$ of the residual N_2O due to N_2O reduction, is related to $r_{\text{N}_2\text{O}}$ (Jinuntuya-Nortman et al., 2008; Menyailo and Hungate, 2006; Ostrom et al., 2007; Well and Flessa, 2009). This approach is also potentially applicable for quantification of $r_{\text{N}_2\text{O}}$ in field conditions (Buchen et al., 2018; Park et al., 2011; Toyoda et al., 2011; Verhoeven et al., 2019; Zou et al., 2014). Its advantage over the ^{15}N gas-flux method lies in its easier and non-invasive application, no need of additional fertilization, and much lower costs. But on the other hand, complexity of the N_2O production pathways with co-occurring N_2O reduction, variability of isotope effects and isotope fractionation associated with diffusion processes can make this estimation imprecise (Lewicka-Szczebak et al., 2015; Lewicka-Szczebak et al., 2014; Yu et al., 2020). Since mostly two processes, mixing and reduction, determine the final N_2O isotopic signature, we need at least two isotopic values to be able to assess both: N_2O mixing proportions of two N_2O production pathways and $r_{\text{N}_2\text{O}}$. Therefore, often applied are the dual isotope plots, also called isotope Mapping approach (Map), *i.e.*, isotopic relations in the space $\delta^{15}\text{N}^{\text{SP}}/\delta^{15}\text{N}$ (SP/N Map) and $\delta^{15}\text{N}^{\text{SP}}/\delta^{18}\text{O}$ (SP/O Map). The SP/N Map has been first applied for agricultural soils by Toyoda et al. (2011). Afterwards many studies utilized this relation to determine N_2O mixing proportions and N_2O reduction (Kato et al., 2013; Wolf et al., 2015; Zou et al., 2014). Later, it was shown that $\delta^{18}\text{O}$ can be also used as a good tracer for N_2O production processes, thanks to high O-exchange during bD resulting in quite stable $\delta^{18}\text{O}$ values for this pathway (Lewicka-Szczebak et al., 2016). Based on this finding the SP/O Map for N_2O interpretation was proposed (Lewicka-Szczebak et al., 2017) and applied in recent studies (Buchen et al., 2018; Ibraim et al., 2019; Verhoeven et al., 2019; Wu et al., 2019). Both SP/N and SP/O Map have been applied jointly for field studies (Ibraim et al., 2019) and showed quite a good agreement in the calculated $r_{\text{N}_2\text{O}}$ and f_{bD} values. However, so far these two approaches were not combined together into a complex three-dimensional

model allowing the calculation of pathways mixing proportions and $r_{\text{N}_2\text{O}}$ based on three isotopic signatures ($\delta^{15}\text{N}$, $\delta^{18}\text{O}$, $\delta^{15}\text{N}^{\text{SP}}$) simultaneously. Development of such a model is a clear current need.

Precise quantification of both, the production pathway proportions and the extent of N_2O reduction with isotope

95 Maps is limited by wide ranges of isotopic signatures reported for individual pathways, the overlapping of these isotopic signatures ranges, variations in substrate isotopic compositions, and variability of fractionation factors associated with N_2O reduction (Toyoda et al., 2017; Yu et al., 2020). Hence, it can be questioned how far we can trust the quantitative results provided by calculations based on isotope Maps. To answer this question comparisons with estimates based on independent methods are needed. The first attempt for comparing $r_{\text{N}_2\text{O}}$ 100 obtained with SP/O Map and ^{15}N gas-flux method in a field case study was performed by Buchen et al. (2018). Due to non-identical treatment (different fertilizer application procedures: needle injection of fertilizer solution for ^{15}N treatments and surface distribution of fertilizer in NA treatments; different sizes of ^{15}N and NA microplots and chambers) and the consequent differences in soil moisture and mineral N, the results of both treatments were difficult to compare, however, the $r_{\text{N}_2\text{O}}$ values obtained indicated clearly the dominance of N_2 105 flux over N_2O flux by both methods. That study also presented analysis of various calculation scenarios applying upper and lower limits for mixing isotopic endmembers values and reduction fractionation factors, which revealed pronounced uncertainty of this calculation approach (Buchen et al., 2018). It was suggested that a further study on validation and uncertainty analysis of the SP/O Map is required with particular attention to identical treatment for both approaches under comparison. Another comparison was performed with archival 110 datasets applying helium incubations as reference method and indicated large uncertainties of the calculations based on the SP/O Map (Wu et al., 2019). The huge uncertainties determined in these studies resulted from the fact that the full range of endmember values and fractionation factors reported in the literature was taken into account. But for particular soils and experimental conditions these ranges might be smaller and uncertainties thus lower. Hence, it is still unsure to which extent the ranges of isotopic fractionation factors determined in 115 laboratory conditions and for pure culture studies are valid for particular experiments. It is not feasible to validate each isotope characteristic separately in field studies, since the pathways are not easily separable and this can be only achieved in controlled laboratory conditions.

While these recent studies indicated severe imprecision associated with the $r_{\text{N}_2\text{O}}$ estimations based on N_2O isotopocule approaches (Buchen et al., 2018; Wu et al., 2019), the suitability of this approach in estimation of 120 $r_{\text{N}_2\text{O}}$ and mixing proportions has never been validated in a systematic study with a reference method. Hence, the idea of this study is to validate the methods based on N_2O isotope Maps and determine their attainable precision by parallel application with the reference method - ^{15}N gas-flux method. We compare the calculated N_2 flux based on the ^{15}N gas-flux method (^{15}N treatment) and N_2O isotope Maps (natural abundance (NA) treatment) in laboratory and field experiments applying identical treatment strategy (meaning identical fertilizer application 125 procedure: fertilizer solution applied with needle injection technique, identical water and fertilizer addition and

identical plots and chamber sizes). Moreover, we present a new three-dimensional isotopocule model (3DI model) based on 3D isotopocule space and provide a validation of its outputs. This is the first attempt to systematically validate the results from N₂O natural abundance isotopic studies (N₂O isotopocule approaches) in laboratory and field conditions.

- 130 Our aim is to (1) validate applicability of N₂O isotopocule approaches for N₂ flux determination, (2) validate applicability of N₂O isotopocule approaches for partition of N₂O producing pathways and (3) to develop best evaluation strategy for interpretation of N₂O isotopic data.

2 Methods

2.1 Field study

- 135 Silt loam soil *Albic Luvisol* from arable cropland of Merklingsen experimental station located near Soest (North Rhine-Westphalia, Germany, 51°34'15.5"N, 8°00'06.8"E) was used (87% silt, 11% clay, 2% sand). The soil density of intact cores was 1.3 g ml⁻¹, pH value 6.8, total C content 1.30%, total N content 0.16%, organic matter content 2.14%. The field was sown with winter rye in September 2015 and mineral under foot fertilization was applied. Our experiments were conducted on experimental plots of a field study on management effects on
140 greenhouse gas fluxes. We selected the 'climate-optimized farm' treatment where a complex cropping rotation of silage maize - winter wheat - faba bean – winter barley – perennial rye had been established since 2010 (Kramps-Alpmann et al., 2017). This treatment was managed by zero-tillage with direct seeding and fertilization was a combination of organic (biogas digestate) and mineral fertilizer where doses were set according to official fertilizer recommendations (Baumgärtel and Benke, 2009). On 13th October in each of the four replicate plots (6
145 * 12 m) we established microplots consisting of aluminum cylinders (length 35cm, diameter 15cm) inserted to 30cm depth into the soil so that 5cm extended above the ground for installation of the flux chamber. Three field campaigns were carried out in November 2015 (F1), March 2016 (F2) and Mai/June 2016 (F3). After each field campaign the cylinders were removed, cleaned and later reinstalled on new locations (on 27 Nov 2015 for F2 sampling and on 28 April 2016 for F3 sampling) for the next field campaign.

- 150 On each replicate plot cylinders were installed pairwise – one for gas flux measurements and one for mineral nitrogen sampling – for 3 treatments – natural abundance (NA), traced nitrate (¹⁵NO₃⁻) and traced ammonium (¹⁵NH₄⁺) – in total 6 cylinders per replicate plot. The distance between each treatment cylinder was at least 2m, pair of cylinders for one treatment were in 0.5m distance.

- At the beginning of the experiment, a fertilizer solution with 240 mg N L⁻¹ as NaNO₃ and 240 mg N L⁻¹ as
155 NH₄Cl was added to the experimental microplots through needle injection technique. Three mL of the fertilizer solution was injected into 72 points using 12 needles inserted subsequently into 6 depths (2.5 - 7.5 - 12.5 - 17.5 - 22.5 - 27.5 cm) from the top to the bottom using peristaltic pump. This strategy was based on previous studies

(Buchen et al., 2016; Wu et al., 2011) and was enhanced by pre-experimental tests to obtain the most homogeneous tracer distribution (Lewicka-Szczebak and Well, 2020). Total fertilization was 20 mg N per kg soil (added as NaNO_3 (10 mg N) and NH_4Cl (10 mg N)) which was equivalent to about 80 kg N per ha.

In total, 216 mL of fertilizing solution was inserted into each microplot which resulted in 3 % increase in water content. For ^{15}N -labelled treatments the ^{15}N content in fertilizing solution was calculated to achieve about 60 atom % ^{15}N in the ^{15}N -labelled N pool. The $^{15}\text{NO}_3^-$ treatment received tracer solution containing 68 atom % ^{15}N and the $^{15}\text{NH}_4^+$ treatment received 64 atom % ^{15}N .

Immediately after fertilizing solution addition, the flux chamber microplots were closed for gas accumulation. Opaque PVC chambers of an area of 1.767 dm^2 and a volume of 2.65 dm^3 were applied with installed valves for sample collection and a fan for gas mixing. The closed chamber method (Hutchinson and Mosier, 1981) was used for N_2O flux measurement. Chambers were closed and sealed with air-tight rubber bands for 120 min and headspace sampling was performed after 40, 80 and 120 min into evacuated crimped 20 mL vials with a 30 mL syringe for gas-flux measurements. Additionally, after 120 min, samples for isotope analysis were collected. For ^{15}N treatments two identical replicates were taken into 12 mL evacuated screw-cup Exetainers® (Labco Limited, Ceredigion, UK) with two combined 15 mL syringes. For the NA treatment, one gas sample was transferred into an evacuated 115 mL crimp-cap vial with a 150 mL syringe.

Each field campaign lasted 5 days. Gas samples were collected once on the first day after fertilization, afterwards twice a day – in the morning and in the evening, and once on the last 5th day in the morning.

The soil sampling microplots were treated identically and used for mineral nitrogen sampling. The soil samples were collected with a Goettinger boring rod with 18 mm outer diameter and 14 mm slots (Nietfeld GmbH, Quakenbrück, Germany). Boreholes were sealed by inserting a closed sand-filled PVC pipe with the same diameter as the bore. For each sampling, three cores were collected and homogenised to one mixed sample each day, hence we performed 5 soil samplings during each campaign. The samples were immediately transported to the laboratory at 6°C and mineral nitrogen extractions were performed on the same day.

2.2 Laboratory incubation

The soil from the experimental field site was used to prepare incubation columns for laboratory incubation. The soil, upper 30cm layer, was collected on the 18.01.2018 from the experimental plot used previously for field campaigns and the incubation was conducted from 19.02.2018 to 05.03.2018. The soil was air dried and sieved at 4 mm mesh size. Afterwards, the soil was rewetted to achieve a water content equivalent to 60 % water-filled pore space (WFPS) and fertilised with 20 mg N per kg soil, added as NaNO_3 (10 mg N) and NH_4Cl (10 mg N). Analogically as in the field study, three treatments were prepared: natural abundance (NA), labelled with ^{15}N nitrate ($^{15}\text{NO}_3$) and labelled with ^{15}N ammonium ($^{15}\text{NH}_4$). For the $^{15}\text{NO}_3$ treatment, NaNO_3 solution with 72 atom % ^{15}N was added and for the $^{15}\text{NH}_4$ treatment, NH_4Cl solution with 63 atom % ^{15}N was added. Then soils were

thoroughly mixed to obtain homogenous distribution of water and fertilizer and an equivalent of 1.69 kg dry soil was repacked into each incubation column with bulk density of 1.3 g cm⁻³.

For each treatment 14 columns were prepared, and half of them received additional water injected on the top of the column (100 mL water added) to prepare two moisture treatments: dry (61 % WFPS) and wet (72 % WFPS).

195 The incubation lasted 12 days. In the meantime, on the 6th day of incubation, water addition on the top of each column was repeated (80 mL water added) to increase the soil moisture in both treatments to ca. 68 % WFPS in the dry treatment and ca. 81 % WFPS in the wet treatment. The WFPS values were controlled during the experiment (Fig. S1). The strategy of adding water on the top of the column to achieve target water content was necessary to allow mixing and compaction at a suitable (low) water content of the soil and thus to optimise
200 homogeneity of water and fertilizer distribution (Lewicka-Szczebak and Well, 2020). The incubation temperature was 20°C. The columns were continuously flushed with a gas mixture with reduced N₂ content to increase the measurements sensitivity (2% N₂ and 21% O₂ in He, (Lewicka-Szczebak et al., 2017)) with a flow of 9 mL min⁻¹. Gas samples were collected daily into two 12 mL septum-capped Exetainers® (Labco Limited, Ceredigion, UK) and one crimped 100 mL vial connected to the vents of the incubation columns. Soil samples
205 were collected 5 times during the incubation by sacrificing one incubation column per sampling event, which was then divided into three subsamples (replicate samples of mixed soil).

2.3 Gas analyses

Measurements of N₂O concentrations in the 20 mL samples were carried out with a gas chromatograph (GC, 2014; Shimadzu, Duisburg, Germany) equipped with an electron capture detector (ECD) and an autosampler
210 (Loftfields Analytical Solutions, Neu Eichenberg, Germany). The analytical precision was around 2%.

Flux rates of total N₂O for field campaigns, *i.e.*, including fluxes from ¹⁵N-labelled and non-labelled sources, were calculated from ordinary linear regression of the four consecutive samples over time using the R package gasfluxes (Fuß, 2015) and the following equation:

$$J_{N_2O} = \frac{dC_{N_2O}}{dt} * \frac{V}{A} \quad (1)$$

215 where J_{N_2O} is the flux rate in µg N₂O-N m⁻² h⁻¹, C_{N_2O} is N₂O mass concentration in µg N m⁻³ corrected by the chamber temperature according to the ideal gas law, t is closing time of the chamber, V is volume of the chamber in m³ and A is covered soil area in m².

For laboratory incubations fluxes were calculated based on the dynamic chamber principle. Correction for the inlet concentration is omitted since the N₂O-free gas mixture was used for flushing :

$$J_{N_2O} = C_{N_2O} * \frac{Q}{A} \quad (2)$$

where J_{N_2O} is the flux rate in $\mu\text{g N}_2\text{O-N m}^{-2} \text{ h}^{-1}$, C is N_2O mass concentration in $\mu\text{g N m}^{-3}$ corrected by the incubation temperature according to the ideal gas law, Q is the gas flow rate through the incubation vessels in $\text{m}^3 \text{ h}^{-1}$, and A is soil area in the incubation vessel in m^2 .

225 The gas samples collected from ^{15}N treatments were analyzed for ^{15}N content with a modified GasBench II preparation system coupled to MAT 253 isotope ratio mass spectrometer (Thermo Scientific, Bremen, Germany) according to Lewicka-Szczebak et al. (2013). In this set-up, N_2O is converted to N_2 during in-line reduction, and stable isotope ratios ^{29}R ($^{29}\text{N}_2/^{28}\text{N}_2$) and ^{30}R ($^{30}\text{N}_2/^{29}\text{N}_2$), of N_2 , of the sum of denitrification products ($\text{N}_2+\text{N}_2\text{O}$) and of N_2O are determined. Based on these measurements the following values are calculated according to the
230 respective equations (after Spott et al. (2006)):

The ^{15}N abundance of ^{15}N -labelled pool (a_p) from which N_2 ($a_{p_N_2}$) or N_2O ($a_{p_N_2O}$) originate is calculated as follows:

$$a_p = \frac{{}^{30}x_M - a_M \cdot a_{bgd}}{a_M - a_{bgd}} \quad (3)$$

The calculation of a_p is based on the non-random distribution of N_2 and N_2O isotopologues (Spott et al., 2006)

235 where ${}^{30}x_M$ is the fraction of $^{30}\text{N}_2$ in the total gas mixture:

$${}^{30}x_M = \frac{{}^{30}R}{1 + {}^{29}R + {}^{30}R} \quad (4)$$

a_M is ^{15}N abundance in total gas mixture

$$a_M = \frac{{}^{29}R + 2 \cdot {}^{30}R}{2(1 + {}^{29}R + {}^{30}R)} \quad (5)$$

a_{bgd} is ^{15}N abundance of non-labelled pool (atmospheric background or experimental matrix)

240 The fraction originating from the ^{15}N -labelled pool (f_p) for N_2 ($f_{p_N_2}$), $\text{N}_2+\text{N}_2\text{O}$ ($f_{p_N_2+N_2O}$) and N_2O ($f_{p_N_2O}$) within the total N of the sample is calculated as follows:

$$f_p = \frac{a_M - a_{bgd}}{a_p - a_{bgd}} \quad (6)$$

The fraction originating from the ^{15}N -labelled pool within the sample (f_{N_2}) is calculated, taking into account the actual N_2 concentration background in the sample C_{N_2} :

$$245 \quad f_{N_2} = f_{p_N_2} * C_{N_2} \quad (7)$$

From the f_{N_2} value determined with Eq.7 the N_2 flux was calculated, in the same manner as for N_2O , for field campaigns (Eq. 1):

$$J_{N_2} = \frac{f_{N_2}}{dt} * \frac{V}{A} \quad (8)$$

where J_{N_2} is the N_2 flux rate in $\mu\text{g } N_2\text{-N m}^2 \text{ h}^{-1}$, f_{N_2} is N_2 mass concentration in $\mu\text{g N m}^3$ corrected by the chamber temperature according to the ideal gas law, t is closing time of the chamber, V is volume of the chamber in m^3 and A is covered soil area in m^2 . Chamber closing time was 120 min and for one chosen field study (F3) the linearity of N_2 increase over 120 min was checked and confirmed. The fluxes correction for underestimation due to subsoil flux and gas soil storage (Well et al., 2019b) was not performed because the focus of this paper was to determine r_{N_2O} while subsoil diffusion of N_2 and N_2O is almost identical. This correction would thus not significantly impact r_{N_2O} . But the fluxes shown in Fig. S2 are measured fluxes and include the underestimation of ^{15}N -based estimates (Well et al., 2019b).

For laboratory incubations with the constant flow through N_2 flux was determined in the same manner as respectively for N_2O (Eq. 2):

$$J_{N_2} = f_{N_2} * \frac{Q}{A} \quad (9)$$

where J_{N_2} is the N_2 flux rate in $\mu\text{g } N_2\text{-N m}^2 \text{ h}^{-1}$, f_{N_2} is N_2 mass concentration in $\mu\text{g N m}^3$ corrected by the chamber temperature according to the ideal gas law, Q is the gas flow rate through the incubation vessels in $\text{m}^3 \text{ h}^{-1}$, and A is soil area in the incubation vessel in m^2 .

N_2O residual fraction (r_{N_2O}) representing the unreduced N_2O mole fraction of total gross N_2O production (Lewicka-Szczebak et al., 2017) is calculated as:

$$r_{N_2O} = \frac{J_{N_2O}}{J_{N_2O} + J_{N_2}} \quad (10)$$

where J_{N_2O} and J_{N_2} are the N_2O and N_2 flux rates in $\mu\text{g } N_2O\text{-N m}^2 \text{ h}^{-1}$.

The analytical detection limit of the calculated N_2 flux from the ^{15}N labelled pool was approx. $50 \mu\text{g N m}^2 \text{ h}^{-1}$ for field studies and approx. $1.5 \mu\text{g N m}^2 \text{ h}^{-1}$ for laboratory experiments (due to increased sensitivity as a result of the N_2 -reduced atmosphere).

The gas samples collected in NA treatments were analyzed for isotopocule N_2O signatures using a Delta V isotope ratio mass spectrometer (Thermo Scientific, Bremen, Germany), coupled to an automatic preparation system with Precon + Trace GC Isolink (Thermo Scientific), where N_2O was pre-concentrated, separated and purified and m/z 44, 45, and 46 of the intact N_2O^+ ions as well as m/z 30 and 31 of NO^+ fragment ions were determined. The results were evaluated accordingly (Röckmann et al., 2003; Toyoda and Yoshida, 1999; Westley et al., 2007) which allows the determination of average $\delta^{15}\text{N}$, $\delta^{15}\text{N}^{\alpha}$ ($\delta^{15}\text{N}$ of the central N position of the N_2O molecule), and $\delta^{15}\text{N}^{\beta}$ ($\delta^{15}\text{N}$ of the peripheral N position of the N_2O molecule) was calculated as $\delta^{15}\text{N} = (\delta^{15}\text{N}^{\alpha} + \delta^{15}\text{N}^{\beta})/2$ and ^{15}N site preference ($\delta^{15}\text{N}^{\text{SP}}$) as $\delta^{15}\text{N}^{\text{SP}} = \delta^{15}\text{N}^{\alpha} - \delta^{15}\text{N}^{\beta}$.

Pure N_2O analysed for isotopocule values in the laboratory of the Tokyo Institute of Technology was used as internal reference gas applying calibration procedures reported previously (Toyoda and Yoshida, 1999; Westley et al., 2007). Moreover, the standards from a laboratory inter-comparison (REF1, REF2) were used for

performing two-point calibration for $\delta^{15}\text{N}^{\text{SP}}$ values (Mohn et al., 2014). All isotopic values are expressed as ‰ deviation from the $^{15}\text{N}/^{14}\text{N}$ and $^{18}\text{O}/^{16}\text{O}$ ratios of the reference materials (i.e. atmospheric N_2 and Vienna Standard Mean Ocean Water (VSMOW), respectively). The analytical precision determined as standard deviation (1σ) of the internal standards for measurements of $\delta^{15}\text{N}$, $\delta^{18}\text{O}$, and $\delta^{15}\text{N}^{\text{SP}}$ was typically 0.1, 0.1, and 0.5 ‰, respectively.

2.4 Soil analyses

All soil samples were homogenized. Soil water content was determined by weight loss after 24 h drying in 110°C . Soil pH was determined in 0.01 mol CaCl_2 solution (ratio 1:5). Nitrate and ammonium concentration was determined by extraction in 2M KCl in 1:4 ratio by 1h shaking. Nitrite concentration was determined in alkaline extraction solution of 2M KCl with addition of 2M KOH (25 mL per L) in 1:1 ratio for 1 minute of intensive shaking (Stevens and Laughlin, 1995). The amount of added KOH was adjusted to keep the alkaline conditions in extracts (pH over 8). After shaking, the samples were centrifuged for 5 minutes and filtrated. The extracts for NO_2^- measurements were stored at -4°C and analyzed within 5 days. NO_3^- , NH_4^+ and NO_2^- concentrations were determined colorimetrically with an automated analyser (Skalar Analytical B.V., Breda, the Netherlands).

To determine isotopic signatures of mineral nitrogen in NA treatments, microbial analytical methods were applied. For nitrate, the bacterial denitrification method with *Pseudomonas aureofaciens* was applied (Casciotti et al., 2002; Sigman et al., 2001). For nitrite, the bacterial denitrification method for selective nitrite reduction with *Stenotrophomonas nitritireducens* was applied (Böhlke et al., 2007), also for ^{15}N -enriched samples from ^{15}N treatments. For ammonium, a chemical conversion to nitrite with hypobromite oxidation (Zhang et al., 2007) followed by bacterial conversion of nitrite after pH adjustment was applied (Felix et al., 2013).

In ^{15}N treatments, ^{15}N abundances of NO_3^- ($a_{\text{NO}_3^-}$) and NH_4^+ ($a_{\text{NH}_4^+}$) were measured according to the procedure described in Stange et al. (2007) and Eschenbach et al. (2017). NO_3^- was reduced to NO by Vanadium-III chloride (VCl_3) and NH_4^+ was oxidized to N_2 by hypobromite (NaOBr). NO and N_2 were used as measurement gas. Measurements were performed with a quadrupole mass spectrometer (GAM 200, InProcess, Bremen, Germany).

2.5 N_2O isotope mapping approach (Map)

The Mapping approach is based on the different slopes of the mixing line between bD (possibly including also nD) and fD or Ni and the reduction line reflecting isotopic enrichment of residual N_2O due to its partial reduction in dual isotope plots. Both lines are defined from the known most relevant literature data on the respective mixing endmembers isotopic signatures and reduction fractionation factors. The detailed isotopic characteristics applied for the isotope Maps are presented in Table 1 and follow the most recent review paper (Yu et al., 2020). The detailed calculation strategy for SP/O Map can be found in the Supplement for the Wu et al. (2019) paper

and for SP/N Map in the Supplement for the Toyoda et al. (2011) paper. The calculations are performed

315 according to two possible cases of N₂O mixing and reduction:

- Case 1 - N₂O produced from bD is first partially reduced to N₂, followed by mixing of the residual N₂O with N₂O from other pathways,
- Case 2 - N₂O produced by various pathways is first mixed and afterwards reduced.

The calculations can be performed following different scenarios of particular endmember mixing: either bD-fD
320 mixing or bD-Ni mixing. For our case studies, due to rather high soil moisture (>60% WFPS) and low ammonium content (Table 2), we rather expect higher fD contribution than Ni, hence the bD-fD mixing was applied and contribution of Ni was neglected. In the supplement, we also present a comparison of calculation results based on both mixing scenarios bD-fD and bD-Ni (Table S1 and supplementary spreadsheet table). This comparison only show pronounced differences for F1 treatment. nD cannot be separated from bD fraction in this
325 approach due to isotope overlap (Fig.1), and the calculated bD fraction may also include nD.

For the graphical presentation of dual isotope plots for sampling points always $\delta^{18}\text{O}$ and $\delta^{15}\text{N}$ values of emitted N₂O are plotted ($\delta^{18}\text{O}_{\text{N}_2\text{O}}$, $\delta^{15}\text{N}_{\text{N}_2\text{O}}$). But the precursors isotopic signatures ($\delta^{18}\text{O}_{\text{H}_2\text{O}}$, $\delta^{15}\text{N}_{\text{NO}_3^-}$, $\delta^{15}\text{N}_{\text{NH}_4^+}$) are taken into account by respective correction of mixing endmembers isotopic ranges (see Table 1). The literature endmember ranges are given as isotope effects (ϵ) expressed in relation to particular precursor relevant for
330 particular pathway:

$$\epsilon_{\text{N}_2\text{O}/\text{precursor}} = \delta_{\text{N}_2\text{O}} - \delta_{\text{precursor}} \quad (11)$$

e.g. for $\delta^{18}\text{O}$ of bD the $\epsilon_{\text{N}_2\text{O}/\text{H}_2\text{O}}$ is calculated by subtracting the precursor isotopic signature ($\delta_{\text{H}_2\text{O}}$) from the measured $\delta_{\text{N}_2\text{O}}$ values, i.e.: $\delta_{\text{N}_2\text{O}} = 10$, $\delta_{\text{H}_2\text{O}} = -9$; $\epsilon_{\text{N}_2\text{O}/\text{H}_2\text{O}} = 19$
335

Afterwards, the literature isotope effects are corrected with the actually measured precursor values determined for the particular study ($\delta_{\text{actual precursor}}$) to determine the characteristic isotopic signature of N₂O emitted from the particular mixing endmember for this particular study conditions ($\delta_{\text{N}_2\text{O, endmember}}$):

$$\delta_{\text{N}_2\text{O_endmember}} = \epsilon_{\text{N}_2\text{O}/\text{precursor}} + \delta_{\text{actual precursor}} \quad (12)$$

340 e.g. for $\delta^{18}\text{O}$ of bD: $\epsilon_{\text{N}_2\text{O}/\text{H}_2\text{O}} = 19$, $\delta_{\text{actual H}_2\text{O}} = -6.4$, $\delta_{\text{N}_2\text{O_bD}} = 12.6$.

Hence, the endmember ranges represent the expected isotopic signatures of N₂O originating from each mixing endmember for the particular case study characterised by specific precursor isotopic signatures. Such approach
345 allows for presenting all data in the common isotopic scales without presumption on the dominating pathway and dominating precursor. Hence, this new approach presented here is actually a further development of Maps, since this allows for correcting both Ni/nD and bD/fD endmembers with relevant distinct precursors, in contrast to only correcting measured values with one common assumed precursor isotopic signature. In previous papers, where $\delta^{18}\text{O}$ and $\delta^{15}\text{N}$ related to precursors ($\delta^{18}\text{O}_{\text{N}_2\text{O}/\text{H}_2\text{O}}$, $\delta^{15}\text{N}_{\text{N}_2\text{O}/\text{NO}_3}$) were plotted (Ibraim et al., 2019; Lewicka-

350 Szczebak et al., 2017; Lewicka-Szczebak et al., 2016) it was assumed that denitrification must be the dominating N₂O production pathway.

Table 1

355 2.6 Three-dimensional N₂O isotopocule model (3DI model)

The probability distributions of proportional contributions f_i were determined using a stable isotope mixing model in the Bayesian framework. This allowed us to integrate three N₂O isotopic signatures into one model to find the nearest solution for the r_{N_2O} and mixing proportions. The core of the model was based on the work of Moore and Semmens (2008) which was further extended with implementation of N₂O reduction in two possible cases (analogically as for Maps – see Section 2.5):

$$\text{Case 1)} \quad f_{bD} (\delta_{bD} + \varepsilon \ln(r_{bD})) + f_{nD} \delta_{nD} + f_{fD} \delta_{fD} + f_{Ni} \delta_{Ni} = \delta_{N_2O} \quad (13)$$

$$\text{Case 2)} \quad f_{bD} \delta_{bD} + f_{nD} \delta_{nD} + f_{fD} \delta_{fD} + f_{Ni} \delta_{Ni} + \varepsilon \ln(r_{N_2O}) = \delta_{N_2O} \quad (14)$$

where f stands for fraction of N₂O originating from a particular pathway and δ stands for isotopic signature characteristic of this pathway, respectively for bD, nD, fD and nitrification Ni. ε is the isotope fractionation factor for N₂O reduction to N₂ and r_{N_2O} is the N₂O residual fraction as defined in Eq. 10. r_{bD} is the N₂O residual fraction of bacterial denitrification only, as it is assumed in Case 1. This value can be recalculated to obtain r_{N_2O} as follows:

$$r_{N_2O} = f_{bD} r_{bD} + f_{nD} + f_{fD} + f_{Ni} \quad (15)$$

Let us briefly summarize the key assumptions and features of the statistical model. The input data of measured m isotope signatures (here three: $\delta^{15}N$, $\delta^{15}N^{SP}$, $\delta^{18}O$) from n sources (here four: bD, nD, fD and Ni) is assumed to be normally distributed and multiple measurements (here: 1 to 7 replicates) constitute a single sample, on which the Monte-Carlo integration is performed. The uncertainties of the sources' data is fed into the model through the variance in the calculation of unnormalized likelihood (see eq. 18). For prior distributions of parameters flat Dirichlet distribution was used for proportional source contributions f_i and uniform distribution for reduction parameter r . For each random sample (f_i , r) a mean and a variance of each isotope signature j are calculated (different for two cases listed above):

$$\text{Case 1)} \quad \mu_j = \sum_{i=1}^n (f_i \delta_{ij}) + f_{bD} \varepsilon \ln(r_{bD}), \sigma_j = \sqrt{\sum_{i=1}^n (f_i \sigma_{ij}^2) + f_{bD} |\ln(r_{bD})| \sigma_{\varepsilon j}^2} \quad (16)$$

$$\text{Case 2)} \quad \mu_j = \sum_{i=1}^n (f_i \delta_{ij}) + \varepsilon \ln(r_{N_2O}), \sigma_j = \sqrt{\sum_{i=1}^n (f_i \sigma_{ij}^2) + |\ln(r_{N_2O})| \sigma_{\varepsilon j}^2} \quad (17)$$

and the likelihood of such a combination is calculated as:

$$L(x | \mu_j, \sigma_j) = \prod_k^N \prod_j^m \left[\frac{1}{\sigma_j \sqrt{2\pi}} \exp \left(\frac{-(x_{kj} - \mu_j)^2}{2\sigma_j^2} \right) \right] \quad (18)$$

where x_{kj} stands for k^{th} measurement of the sample and j^{th} isotope signature. We use the Markov-chain Monte-Carlo with the Metropolis condition: $L_{i+1}/L_i \geq \alpha$, where α is a random variable sampled from a uniform distribution.

The detailed input parameters for the model are presented in Table 1. The detailed isotopic characteristics to be applied for the isotope signatures of mixing endmembers and reduction fractionation factors are adopted after the most recent review paper (Yu et al., 2020).

2.7 Statistics

For results comparisons, an analysis of variance was used with the significance level α of 0.1. The uncertainty values provided for the measured parameters represent the standard deviation (1σ) of the replicates. The propagated uncertainty was calculated using Gauss' error propagation equation taking into account standard deviations of all individual parameters.

The agreement with the reference method was assessed with the Nash–Sutcliffe efficiency (F) (Nash and Sutcliffe, 1970), which represent the R of the fit to the 1:1 line between observed reference (O) and estimated (E) values, as also used in previous validation studies (Lewicka-Szczebak et al., 2017; Wu et al., 2019):

$$F = 1 - \frac{\sum_{i=1}^n (O_i - E_i)^2}{\sum_{i=1}^n (O_i - O)^2} \quad (19)$$

where E_i is the $r_{\text{N}_2\text{O}}$ value estimated with the method under validation, corresponding to the observed $r_{\text{N}_2\text{O}}$ value determined with the reference method: O_i , and O is the observed mean. In this assessment, an $F=1$ refers to a perfect fit between estimated and reference values, lower F values indicate worse model fits, whereas a negative F occurs when the observed mean is a better predictor than the model.

3. Results

3.1 Soil properties

Soil organic N was analyzed in soil samples from each sampling campaign and varied only slightly with content of 0.141 ± 0.007 % N and isotopic signature $\delta^{15}\text{N}$ of $7.4 \pm 0.4\text{‰}$. $\delta^{18}\text{O}$ of soil water varied only slightly for field campaigns and equaled -6.7 ‰ for F1, -7.0 ‰ for F2, and -6.4 ‰ for F3, but was higher for incubation experiments with mean of -5.3 ‰. Detailed characteristics for mineral nitrogen contents and isotopic signatures are presented in Table 2. The variations in water and nitrate content during the field campaigns and laboratory incubations with comparison between NA and ^{15}N treatment are presented in the supplement (Fig. S1). Importantly, for vast majority of sampling points these soil conditions are well comparable between both

treatments which allows for the methods comparison. Significant difference was only noted for nitrate content
410 for the last sample in L2 and for water content for the last sample in F1 (Fig. S1).

3.2 Field campaigns

The first field campaign F1 in Nov 2015 (23rd Nov-27th Nov) showed low N₂O fluxes from 1.2 to 33.2 g N-N₂O
ha⁻¹ d⁻¹ (Table 2). N₂O isotopic signatures were determined for all the samples except one. The N₂ fluxes were
under the detection limit for all samples, i.e. below 11 g N-N₂ ha⁻¹ d⁻¹. In this case, the reference r_{N_2O} values form
415 the ¹⁵N treatment could not be precisely determined. However, from the information that N₂ flux is below the
detection limit even for the highest N₂O fluxes observed we can assess that r_{N_2O} must be higher than 0.75. For
F1, soil temperature varied from 1.6 to 8.6 °C, mean 4.1 °C, WFPS varied from 54.1 to 72.4 %, mean 65 %.

The second field campaign F2 in March 2016 (7th March-11th March) showed very variable N₂O fluxes from 0.5
to 110.7 g N-N₂O ha⁻¹ d⁻¹. N₂O isotopic signatures could be determined only in 17 samples from 26. The N₂
420 fluxes were above the detection limit for 15 samples from 26, and varied from 23 to 304 g N-N₂ ha⁻¹ d⁻¹. In this
case, the reference r_{N_2O} values from the ¹⁵N treatment could be determined for 4 sampling dates out of 8. For F2,
soil temperature varied from 1.4 to 12.0 °C, mean 6.4 °C, WFPS varied from 57.9 to 77.9 %, mean 69 %.

The third field campaign F3 in Mai/June 2016 (30th Mai-3rd June) showed very high N₂O fluxes from 1 to 1471 g
N-N₂O ha⁻¹ d⁻¹. N₂O isotopic signatures could be determined in all samples. The N₂ fluxes were always above the
425 detection limit and varied from 114 to 2060 g N-N₂ ha⁻¹ d⁻¹. In this case, the reference r_{N_2O} values from the ¹⁵N
treatment could be determined for all 8 sampling times. For F3, soil temperature varied from 17.0 to 32.5 °C,
mean 21.4 °C, WFPS varied from 52.1 to 72.0 %, mean 62 %.

The detailed variations in gas fluxes during field campaigns and variations in ¹⁵N abundance in various pools
(a_{NO_3} , $a_{P_N_2O}$ and $a_{P_N_2}$) and the N₂O ¹⁵N-pool derived fraction ($f_{P_N_2O}$) are presented in the supplement (Fig. S2
430 C-E and Fig. S3 C-E). There are no significant differences in N₂O flux between ¹⁵N and NA treatment (Fig. S2
C-E). In F3 the fluxes were much larger than in F1 and F2 and were decreasing during the sampling campaign,
whereas N₂ flux was very variable and showed large differences between repetitions, represented by large error
bars (Fig. S2 E). In F1 and F2 the ¹⁵N-pool derived fraction was significantly lower when compared to F3. In F3
 $a_{P_N_2}$ and $a_{P_N_2O}$ was comparable and higher than a_{NO_3} in the first three samples and similar with a_{NO_3} for the last
435 5 samples. In F2 $a_{P_N_2O}$ strictly depended on a_{NO_3} and both showed clear decreasing trend, whereas $a_{P_N_2}$ was
determined only in two sampling points and was significantly lower than $a_{P_N_2O}$ and a_{NO_3} .

3.3 Laboratory experiments

The laboratory experiment L1 was conducted in dryer conditions than L2. In L1 initially WFPS was about 60 % and after water addition (9th day of the experiment) it was increased to 65%. In L2 initially WFPS was about 70 % and after water addition (9th day of the experiment) it was increased to 80 %.

N₂O fluxes in L1 were quite low from 0.2 to 16.7 g N-N₂O ha⁻¹ d⁻¹. N₂O isotopic signatures could be determined in 38 from 56 samples. The N₂ fluxes were above the detection limit only for 43 from 112 samples and varied from 1.5 to 69.4 g N-N₂ ha⁻¹ d⁻¹. In this case the reference r_{N_2O} values from the ¹⁵N treatment could only be determined for 7 sampling times out of 10. In L2 N₂O fluxes were higher and varied in wide range from 0.4 to 297.4 gN-N₂O ha⁻¹ d⁻¹. N₂O isotopic signatures could be determined in 40 from 56 samples. The N₂ fluxes were above the detection limit only for 87 from 112 samples and varied from 1.2 to 199 g N-N₂ ha⁻¹ d⁻¹. In this case, the reference r_{N_2O} values from the ¹⁵N treatment could be determined for 9 sampling times out of 10.

The detailed variations in gas fluxes during laboratory incubations and variations in ¹⁵N abundance in various pools (a_{NO_3} , $a_{P_N_2O}$ and $a_{P_N_2}$) and the N₂O ¹⁵N-pool derived fraction ($f_{P_N_2O}$) are presented in the supplement (Fig. S2 A-B and Fig. S3 A-B). We often observe significantly different fluxes for NA and ¹⁵N treatment: for L1 only for 2 samples (4 and 5) NA treatment show significantly higher N₂O flux but for L2 majority of sampling points show significantly higher N₂O flux in ¹⁵N treatment, particularly for the last 4 sampling points, after the water addition (Fig. S2 B). Importantly, water content did not differ for this sampling points. In L1 the ¹⁵N-pool derived fraction was significantly lower when compared to L2. In both L1 and L2 $a_{P_N_2}$, $a_{P_N_2O}$ and a_{NO_3} show comparable ranges and only very slight decreasing trend (Fig. S3 A-B).

Table 2

3.5 Maps

SP/O Map

Fig. 1

The majority of isotope results presented in the SP/O Map (Fig.1) is situated within the area limited by reduction and mixing lines, which allows for application of the calculation approach based on SP/O Map. Numerous samples, mostly from the laboratory incubation studies, are situated below the mean reduction line but within the minimum reduction line. For these samples, the calculation results provide f_{bD} values slightly above 1, which are

set for 1 for the further summaries. All calculations and results can be followed in the spreadsheet file in supplementary materials.

470 The endmembers isotope values applied here (after Yu et al. (2020)) differ for nitrification $\delta^{18}\text{O}$ when compared to previous applications of SP/O Map (Buchen et al., 2018; Ibraim et al., 2019; Lewicka-Szczebak et al., 2017; Verhoeven et al., 2019). The currently applied $\delta^{18}\text{O}$ endmember values for Ni ($23.5 \pm 2.1\%$) are lower than previously applied range (from 38.0 to 55.2 ‰, mean 43.0 ‰) and thus result in a separation of Ni and fD, which was not possible in the previous studies. With the current values, we have two possible mixing lines (bD-Ni and bD-fD), whereas in previous studies only one mixing line was applied (bD-(Ni+fD)). This requires the choice of most appropriate mixing scenario for the particular case study. For this study, the results obtained for $r_{\text{N}_2\text{O}}$ and f_{bD} differ mostly only very slightly for both mixing scenarios (see supplementary material, Table S1 and spreadsheet file), which is due to high f_{bD} . For F3, where f_{bD} is near 1, the difference in $r_{\text{N}_2\text{O}}$ does not exceed 0.02, and for F1 with the lowest f_{bD} of ca. 0.7, the difference in $r_{\text{N}_2\text{O}}$ reaches 0.22 (Table S1). Below we summarize the results of calculations assuming bD-fD mixing scenario only.

The calculation has been performed with two cases (see Section 2.5) and all results are shown and compared with reference method in Table 3 and 4. Due to quite high f_{bD} for our study the both cases show only very slight differences (Table 3, Table 4). For the field study F1 we obtained the highest $r_{\text{N}_2\text{O}}$ values (0.86 ± 0.12) and the lowest f_{bD} values (0.74 ± 0.07). For field study F2, the $r_{\text{N}_2\text{O}}$ values were lower (0.38 ± 0.05) and the f_{bD} values were higher (0.92 ± 0.04). For field study F3 the $r_{\text{N}_2\text{O}}$ values were very similar as in F2 (0.33 ± 0.07) and the highest f_{bD} values were noted (0.99 ± 0.01). For the laboratory incubation studies we obtained slightly lower ($p=0.086$) $r_{\text{N}_2\text{O}}$ for L1 (0.19 ± 0.03) when compared to L2 (0.27 ± 0.12). Both laboratory treatments showed very high f_{bD} for L1 (0.99 ± 0.01) and L2 (0.98 ± 0.04).

490 3.6 SP/N Map

Fig.2

For the SP/N Map we present the literature endmember values in relation to the respective precursor, i.e. NO_3^- for bD and fD and NH_4^+ for nD and Ni (Table 1). For the field and laboratory studies, separate mean values for NO_3^- (11.9 and 4.5 ‰ respectively) and NH_4^+ (41.4 and 79.3 ‰, respectively) were applied. These precursor isotopic signatures are the means of 5 samplings for each campaign and experiment. The extremely ^{15}N enriched $\delta^{15}\text{N}_{\text{NH}_4}$ values result in large shift of endmember ranges for nD and Ni. These ranges are ^{15}N depleted in relation to bD when assuming identical $\delta^{15}\text{N}$ values for NO_3^- and NH_4^+ , according to most previous studies (Ibraim et al.,

2019; Koba et al., 2009; Toyoda et al., 2011). But in the case of our experiments, conversely, N₂O originating from nD and Ni would be significantly enriched in ¹⁵N when compared to bD and fD (Fig. 2). For the samples the measured bulk $\delta^{15}\text{N}_{\text{N}_2\text{O}}$ is plotted.

The majority of the samples is located outside the area limited by reduction and bD-fD mixing lines, which mostly precludes the application of calculation approach based on SP/N Map. The separation of mixing and reduction processes is not possible based on this plot, since the slopes of reduction line and bD-Ni mixing line are too similar, especially for laboratory experiments (Fig. 2B).

Another approach to include N precursors values is to apply the individual endmembers isotopic signatures for each N₂O sample by interpolating the measured isotopic signatures of NO₃⁻ and NH₄⁺. With 5 measurements of mineral N isotopic signatures per experiment we get quite a good resolution of these values. Since they show quite high variations (Table 2) applying individual values is a better approach. But still, also by this approach the majority of samples show values out of the calculation range and the results are very ambiguous representing the whole range of possible variations in both $r_{\text{N}_2\text{O}}$ and f_{bD} values. Therefore these values are not summarized here.

3.7 O/N Map

Fig.3

For O/N Map (Fig.3) the $\delta^{18}\text{O}$ values for bD, fD and nD are expressed in relation to soil water and the $\delta^{15}\text{N}$ values for bD and fD in relation to soil NO₃⁻ and for nD and Ni in relation to soil NH₄⁺ (Table 1). For these graphs, it is difficult to determine the reduction-mixing area because the slope of the reduction line is almost identical to the bD-fD mixing line.

A significant linear correlations has been found both for the field and laboratory studies, with $R^2=0.27$ ($p<0.1$) and $R^2=0.40$ ($p<0.01$), respectively. Both correlations show similar linear equations: $\delta^{18}\text{O} = 0.24 * \delta^{15}\text{N} + 33.3$ and $\delta^{18}\text{O} = 0.28 * \delta^{15}\text{N} + 41.6$, for field and laboratory studies, respectively (Fig. 3).

3.8 3DI model

The application of Maps applying $\delta^{15}\text{N}$ data, *i.e.*, SP/N and O/N Map, is very imprecise for this case study due to untypically high $\delta^{15}\text{N}_{\text{NH}_4}$ values and shifted location of the nD and Ni mixing endmembers (Fig. 2, Fig. 3) when compared to cases when similar $\delta^{15}\text{N}_{\text{NH}_4}$ and $\delta^{15}\text{N}_{\text{NO}_3}$ values are determined or assumed. However, still the $\delta^{15}\text{N}$ data comprise important information, which can assist in processes identification when applied jointly with the SP/O Map. Therefore, we combined all the information in one 3DI model where all three isotopic signatures are taken into account.

The results of this model regarding r_{N_2O} are mostly well comparable to the values obtained with SP/O Map (Table 3). However, whereas for SP/O Map both Case 1 and Case 2 provide similar results for r_{N_2O} , for 3DI model these differ more pronouncedly. On the bar plots (Fig. 4) we summarize the results obtained from both modeling cases and below we summarize the results of Case 2, which provides more reliable results, as further discussed (see Section 4.2).

We get much more detailed estimation regarding mixing proportions with 3DI model when compared to the SP/O Map. The dominating N_2O production pathway is clearly bD, which contributes in N_2O production from 46 % for F2 up to 69 % for L2 (Fig. 4). An important role plays also nD contributing from 15% for L2 up to 40% N_2O for F3; low f_{nD} of 4% was found for F1. The f_{iD} is quite variable from 6% for F3 to 26% for F1. N_i shows the lowest contribution around 3-5%, and only slightly higher f_{Ni} of 13% was found for F2 (Fig. 4). N_2 fluxes are highly variable between the experiments, *i.e.*, mean r_{N_2O} values vary from 0.21 for L1 to 0.89 for F1 (Fig. 4, Table 3).

Fig. 4

The model provides very detailed information on probability distribution of the results, which is presented on the matrix plots prepared after Parnell et al. (2013) (supplement, Fig. S4), where histograms of probability distribution of r_{N_2O} and mixing proportions, correlations between the modeled fractions and R coefficients of these correlations are presented (Fig.S4). This summary provides an overview of the reliability of the model outputs and allows for identifying unavoidable model inadequacy. For all the modeled random samples we observe very strong negative correlation between f_{bD} and f_{nD} , similar for both cases, from -0.28 to -0.93, mean -0.63, and between f_{bD} and f_{iD} from -0.15 to -0.97, mean -0.74. r_{N_2O} for Case 2 is always correlated negatively with f_{bD} from -0.15 to -0.84, mean -0.62, and positively with f_{iD} from 0.18 to 0.82, mean 0.62. For Case 1 this correlation is extremely variable for r_{N_2O}/f_{bD} from -0.67 to 0.85 and for r_{N_2O}/f_{iD} from -0.72 to 0.69. The lowest correlation coefficients are noted for f_{Ni} , where mean values never exceed 0.4. This is reflected in the determined ranges of possible results presented in the histograms. f_{Ni} range is typically much narrower than f_{bD} and f_{nD} ranges.

The correlations and histograms vary between the particular campaigns with some typical features.. For F1 we observe a very similar output for Case 1 and Case 2, quite narrow ranges of results and no extremely high correlations. For F2 the ranges are much larger and high negative correlations f_{bD} / f_{nD} and f_{iD} / f_{Ni} indicate possible imprecision in separation of these pathways, which results in much wider range of probable results. For F3 the most extreme negative correlation f_{bD} / f_{nD} is noted, and for Case 1 also r and f_{nD} shows very strong correlation, which may affect the proper estimation of r_{N_2O} . For L1 and L2 we observe lower correlation f_{bD} / f_{nD}

but higher f_{bD} / f_{fD} which is probably a result of different $\delta^{15}\text{N}$ endmember values for nD and Ni and better separation of these pathways. The strong positive correlation of $r_{\text{N}_2\text{O}}$ and f_{bD} for Case 1 in L1, F2 and F3 is rather a logical consequence of the assumptions underlying the Case 1 approach.

3.9 Comparison of $r_{\text{N}_2\text{O}}$ with independent estimates

The N_2O reduction progress calculated with the above presented SP/O Map and 3DI model were compared with the results from the ^{15}N gas-flux method. In the tables below we present the detailed comparison with the results applying both calculation cases (Case 1 and Case 2) for $r_{\text{N}_2\text{O}}$ (Table 3) and for mixing proportions (Table 4).

Table 3

The ranges and the mean values of the replicates means of all sampling dates are quite well comparable for SP/O Map and 3DI model Case 2. Most inconsistent results are obtained in Case 1 of 3DI model, however, for L2 this case seem to be most accurate.

Since the variations of $r_{\text{N}_2\text{O}}$ values in the experiments are very variable in time just a comparison of overall mean values is not informative, we need to compare the temporal changes of $r_{\text{N}_2\text{O}}$ (Fig. 5).

Fig.5

Most extreme changes in time are reported for the laboratory experiment L2 where a very sudden change in $r_{\text{N}_2\text{O}}$ was observed as a consequence of water addition (between sampling 5 and 6). All three estimates present the same trend as the reference method, however, with lower amplitude of the temporal change (Fig. 5B). For field study F3 ^{15}N treatment indicates a constant decrease in $r_{\text{N}_2\text{O}}$, which is only partially reflected in SP/O Map and not at all in 3DI model results. F1 and F2 data are not complete due to N_2 fluxes under detection limit for the whole F1 sampling and half of the samples of F2 campaign. However, for this missing data we can make estimates of the $r_{\text{N}_2\text{O}}$ based on the known detection limit for N_2 flux. We estimated the $r_{\text{N}_2\text{O}}$ values for the missing points assuming the possible N_2 flux: from 0 up to detection limit of $11.3 \text{ gN N}_2 \text{ ha}^{-1} \text{ d}^{-1}$.

Fig.6

In Fig. 6 we checked the fit of $r_{\text{N}_2\text{O}}$ values determined by ^{15}N gas-flux and 3DI model (Fig. 6A) or SP/O Map (Fig. 6B). When analysing all the individual sampling dates or all experiments, the fit to 1:1 line is not very well, especially for many dates of the L2 experiment $r_{\text{N}_2\text{O}}$ is largely underestimated with isotopocule approaches. This

is mostly due to the sudden change in $r_{\text{N}_2\text{O}}$ as presented above (Fig. 5B). But when we compare the means of the whole experiment or the experimental phases before and after water addition for L1 and L2 (red points in Fig. 6), the fit is much better with all points within the error of 0.15 for 3DI model. For SP/O Map the L2 mean after irrigation still shows larger disagreement.

The agreement between isotopocule methods and reference method was statistically checked with F value (Eq. 19). The results for all means, minimal and maximal values are shown in Table 3. The statistically significant agreement was indicated for SP/O Map ($p < 0.1$) and Case 2 of 3DI model ($p < 0.05$), whereas Case 1 of 3DI model shows no agreement. Particular F values calculated with all sampling dates means indicate no significant agreement ($F = 0.13$ for F3, $F = 0.45$ for L1, $F = 0.28$ for L2 – values for fit between Case 2 of 3DI model and reference method), which reinforces the observation based on Fig. 6, that only mean experimental values show good agreement with the reference method, but not the individual samplings.

3.10 Comparison of mixing proportions with independent estimates

The mixing proportions obtained by different approaches are much more complex to compare than $r_{\text{N}_2\text{O}}$ due to the fact that each approach provides distinct information.

- With the reference method – ^{15}N gas-flux – we determine the ^{15}N -pool derived fraction of N_2O ($f_{\text{P}_\text{N}_2\text{O}}$), hence for the $^{15}\text{NO}_3^-$ treatment this is the fraction of N_2O originating from the labeled $^{15}\text{NO}_3^-$ pool. Theoretically, this can be bD or fD. It was intended to use the $^{15}\text{NH}_4^+$ treatment for the determination of N_2O fraction derived from NH_4^+ pool but due to rapid NH_4^+ turnover into NO_3^- , we deal with a highly ^{15}N -labeled NO_3^- pool in the $^{15}\text{NH}_4^+$ treatment and hence are not able to precisely separate these pools (results not shown).
- With SP/O Map we determine the f_{bD} fraction. But since in the SP/O Map bD and nD cannot be distinguished due to overlapping isotopic signatures (Fig. 1) this fraction actually informs about bD+nD fraction.
- With the 3DI model we are able to theoretically determine most of the fractions contributing to the N_2O flux, but the precision of such determination depends on the isotopic separation of particular pathways in 3D isotopocule plot. In our case study this separation is not very good, especially for $\delta^{15}\text{N}$ (see Section 3.6 and 3.7), hence this determination is associated with pronounced uncertainty (Fig. S4).

To compare all this results we present a comparison $f_{\text{P}_\text{N}_2\text{O}}$ of ^{15}N gas-flux (representing bD+fD) with f_{bD} of SP/O Map (representing bD+nD) and respective results (f_{bD} , $f_{\text{bD+fD}}$, $f_{\text{bD+nD}}$) of the 3DI model (Fig. 7, Table 4).

Table 4

Fig. 7

The reasonable agreement in the ranges of values is obtained for experiments L1, L2 and F3, but a large disagreement with the reference ^{15}N gas-flux method is observed for field studies F1 and F2 (Table 4). For these studies, extremely low $f_{\text{p-N}_2\text{O}}$ was found by the ^{15}N gas-flux method, of 0.28 and 0.23, respectively. The time dynamics are not very well reflected by various approaches (Fig.7). This is mostly visible in F3 (Fig. 7E) where the f_{bD} and $f_{\text{bD+nD}}$ show large variations between samplings from below 0.1 to above 0.9. These rapid changes show much lower amplitudes according to the ^{15}N gas-flux approach. The contribution of $f_{\text{bD+nD}}$ determined by the 3DI model as well as f_{bD} determined by the SP/O Map are much more stable in time, which is especially clear for F3 (Fig. 7E), but also true for other campaigns (Fig.7).

For the mixing proportions the statistical agreement with F value (Eq. 19) cannot be determined because the fractions provided by various approaches do not precisely refer to the identical pathways contributions and are not directly comparable.

4. Discussion

4.1 Mapping approaches for N_2O data interpretation – opportunities and limitations

So far the interpretations of N_2O isotope data are most commonly done with dual isotope plots. Whereas SP/N and O/N plots were applied in numerous studies before (Kato et al., 2013; Koba et al., 2009; Opdyke et al., 2009; Ostrom et al., 2007; Ostrom et al., 2010; Toyoda et al., 2011; Well et al., 2012; Yamagishi et al., 2007; Zou et al., 2014) the usage of the SP/O plot is quite a new idea (Lewicka-Szczebak et al., 2017), but already used for field studies (Buchen et al., 2018; Ibraim et al., 2019; Verhoeven et al., 2019). The recent work basing on archival datasets with independent estimates of N_2 flux showed some weak accordance of the results of the SP/O Map with independent estimates (Wu et al., 2019). However, the reasons are difficult to identify for archival data. Here we present the performance of mapping approaches validated with independent estimates based on ^{15}N gas-flux method and try to identify potential problems.

The first challenge, especially for field studies, is obtaining complete datasets. This is due to limited sensitivity of the isotopic measurements and a need for sufficient N_2O and N_2 flux. For our first field study (F1), N_2 flux was under the detection limit and the $r_{\text{N}_2\text{O}}$ values can thus not be fully compared. For the F2 field study we have numerous missing data due to N_2O or N_2 flux under detection limit, hence only a limited number of data can be compared. This may be the main reason (besides other discussed later – Section 4.4) for the weakest accordance of the results for F2. For this field study only four samples showed the N_2 flux above the detection limit and these measured N_2 fluxes associated with the low N_2O fluxes yield very low $r_{\text{N}_2\text{O}}$ values. For samples with N_2

flux below the detection limit the estimated $r_{\text{N}_2\text{O}}$ ranges show possibly also much higher values (Fig. 5D). Hence, possibly by missing the measurements of low N_2 fluxes we miss the higher $r_{\text{N}_2\text{O}}$ values and our calculated means are not representative for the whole experiment (Table 3).

SP/O Map

The SP/O Map was proposed (Lewicka-Szczebak et al., 2017) after it was found that $\delta^{18}\text{O}$ of the N_2O produced by bacterial and fungal denitrification is quite stable and together with SP may be useable for discrimination of these pathways (Lewicka-Szczebak et al., 2016; Rohe et al., 2014a). As O-precursor for bD, fD and nD the soil water is accepted, under the assumption of nearly complete O-exchange between water and denitrification intermediates. The high extent of O-exchange during denitrification has been confirmed experimentally (Kool et al., 2009; Lewicka-Szczebak et al., 2016; Rohe et al., 2014b) and it results in a quite stable range for mixing endmember values for $\delta^{18}\text{O}$ for bacterial and fungal denitrification (Fig. 1). Importantly, due to higher isotope fractionation effect associated with subsequent reduction steps of NO_3^- to N_2O (i.e. removal of oxygen atoms, so called branching effect) during fungal denitrification, the ranges for $\delta^{18}\text{O}$ of bacterial and fungal N_2O differ significantly (Lewicka-Szczebak et al., 2016). Fungal denitrification shows very consequent high O-exchange and high fractionation during O-branching (Rohe et al., 2014b; Rohe et al., 2017), whereas bacterial denitrification is characterized in general by lower fractionation, but the differences in both fractionation and O-exchange between particular bacterial strains are large (Rohe et al., 2017). As a result of lower O-exchange showed by some bacterial strains, $\delta^{18}\text{O}_{\text{NO}_3^-}$ is also incorporated into produced N_2O (Rohe et al., 2017). This complicates the application of the proposed SP/O Map. It is not clear how large is the importance of such bacterial strains characterized by low O-exchange in soil communities. We assume it must be low, because soil incubation studies indicated so far mostly very high exchange rates (Kool et al., 2007; Kool et al., 2009; Lewicka-Szczebak et al., 2016). These studies covered in total 16 soils and only for two forest soils characterized by very low N_2O emission the O-exchange was around 20 % (Kool et al., 2009), otherwise over 60 %, with mean of around 90 % (Kool et al., 2009; Lewicka-Szczebak et al., 2016). Importantly, the range of $\delta^{18}\text{O}$ values determined for bacterial denitrification does not assume complete O-exchange but is determined for the soil samples of O-exchange varying in the range from 63 to 100% (Lewicka-Szczebak et al., 2016). Hence, based on current knowledge, this can be assumed typical for most soils and experimental conditions. Also in this study, quite a good agreement of the $r_{\text{N}_2\text{O}}$ determined by the O/SP Map and the reference method (see Section 3.9) allows us to confirm the general assumption underlying this calculation method.

SP/N Map

The application of dual isotope plot SP/N was initially proposed by Yamagishi et al. (2007) for ocean waters and by Koba et al. (2009) for groundwater studies. In open water bodies, the application of SP/N Map might be

effective due to relatively homogenous distribution of substrates in the sampled water volume and thus not biased by the spatial heterogeneity in ^{15}N enrichment that can occur in soils due to the fractionation processes in soil microsites (Bergstermann et al., 2011; Cardenas et al., 2017; Castellano-Hinojosa et al., 2019; Lewicka-Szczebak et al., 2015; Well et al., 2012). The $\delta^{15}\text{N}$ isotopic signatures of samples were corrected for NO_3^- substrate only and for water studies this approach was well justified by the complete conversion of NH_4^+ to NO_3^- (Koba et al., 2009). This assumption was based on the low NH_4^+ concentration and should result in equal $\delta^{15}\text{N}$ of NH_4^+ and NO_3^- , which allowed to put the whole data into a single $\delta^{15}\text{N}^{\text{SP}} - \delta^{15}\text{N}$ scheme. But for soil studies, due to multiple possible N substrates and difficulties to find a proper correcting strategy, later studies rather applied bulk measured $\delta^{15}\text{N}$ without corrections (Kato et al., 2013; Toyoda et al., 2011). Up to now, the most appropriate approach of taking precursors into account is the recalculation of literature mixing endmember values to the actually measured substrate values for each particular pathway, namely NO_3^- for denitrification and NH_4^+ for nitrification (Zou et al., 2014). But this approach was not successful for this study (see Section 3.6). When endmember mixing areas were recalculated with the measured substrate isotope signatures, most of the sampling points were located outside the mixing-reduction area. This is most probably due to large variations in isotopic signatures of the substrates and the fact that the analyzed bulk $\delta^{15}\text{N}$ values are not representative for the actually utilized substrate pools due to spatial heterogeneity of fractionating processes as outlined above. Moreover, the range of values for NH_4^+ and NO_3^- of our studies resulted in a very untypical location of endmember ranges for denitrification and nitrification on the Maps (Fig. 2, Fig. 3), hence the method is not really suitable for discriminating mixing of these pathways and N_2O reduction for this particular study. This is due to the extremely high $\delta^{15}\text{N}_{\text{NH}_4}$ values (even up to 100‰) which are associated with low NH_4^+ contents (Table 2). This indicates that the ammonium pool was highly fractionated and nearly exhausted. This fast ammonium consumption will be further investigated in the follow up paper applying Ntrace model, where we also apply the $^{15}\text{NH}_4$ treatment for its proper interpretation (Müller et al., 2014).

O/N Map

After it was observed that N_2O reduction results in the typical O/N slope of 2.6 (Menyailo and Hungate, 2006; Ostrom et al., 2007; Well and Flessa, 2009) the O/N Map was proposed for identification of significant N_2O reduction based on the observed slope higher than 1 (Opdyke et al., 2009; Ostrom et al., 2007). However, it must be noted that in case of temporal shifts in the isotopic composition of the N or O substrate the assessment of the importance of N_2O reduction is not valid (Ostrom et al., 2010). This approach was well suited for short term controlled experiments, however for longer field studies, where we deal with large variations of N substrates isotopic signatures, application of this approach appears problematic. We plotted our data in the O/N Map and found a significant linear relationship for field and laboratory studies, both with a very similar equations. The observed slopes of 0.24 and 0.28, respectively, are much below 1, although the N_2O reduction shows important

contribution for these experiments (Table 3). Hence, this observed slope is rather due to change of active substrate pool or changes in the isotopic fractionation (Cardenas et al., 2017). This might be a result of changes in soil moisture during experiments (irrigation or rain episodes). The observed shift in $\delta^{15}\text{N}$ is ca. four times larger than for $\delta^{18}\text{O}$. We suppose that water addition intensified N_2O production and this might have caused significant enrichment in active nitrate pool in soil microsites. For O isotopes intensified N_2O production may result in slightly lower O-exchange, which may increase the $\delta^{18}\text{O}$ values as a result of incorporation of nitrate O signature (Lewicka-Szczebak et al., 2015; Rohe et al., 2017). Consequently, the isotope effects due to reduction are significantly interfered by shifts in N_2O precursors dynamics. Since for this Map both N and O isotopes depend on the precursor isotopic signature and are significantly altered by the diffusion (Well and Flessa, 2008), the interpretations based on this Map are the most ambiguous.

4.2 Three-dimensional N_2O isotopocule model – perspectives of this new approach

Such a model for interpretation of N_2O isotopic data is proposed here for the first time. This model is based on the Bayesian mixing models being well established and widely applied method in food-web studies to partition dietary proportions (Parnell et al., 2013; Phillips et al., 2014). But for N_2O the determination of mixing proportion of different pathways contributing to N_2O production is further complicated by N_2O reduction which alters the final N_2O isotopic signature. This additional parameter was incorporated into the model equations (eq. 13, 14). Moreover, it is still not clarified, if the reduction of N_2O produced during bacterial denitrification only is possible (Case 1) or also N_2O from other pathways can be further reduced by bacterial denitrifiers (Case 2), hence both cases need to be considered. The model has a few advantages over the SP/O Map. First of all, it allows for including uncertainties of input data into the model and allows for assessment of the confidence intervals for the results. Moreover, theoretically the 3DI model allows for separation of four N_2O production pathways, currently identified as the most relevant, within them f_{ID} , which is so far not distinguishable with other isotopic methods (Wrage-Mönnig et al., 2018).

For our case studies, it has been shown that $\delta^{15}\text{N}$ values are not useful in dual isotope plots for quantitative estimations (Fig.2, Fig.3, Section 3.6 and 3.7) but are helpful to constrain mixing proportions when incorporated into the 3DI model. Since the model bases on probability distribution, it allows for providing estimates even for imprecise data, e.g. as in our case by difficulties in proper determination of $\delta^{15}\text{N}$ endmember ranges due to very unstable precursor isotopic signatures.

The model outputs allow us to assess the quality of model performance and reliability of the results (Fig. S4, Section 3.8). From the uncertainty analysis provided by the model, we can determine the confidence intervals for the estimated values (Fig. 5, Fig. 7). This is a total uncertainty resulting from all possible uncertainty sources due to: ranges of endmember values and fractionation factors, variations in N_2O isotopic signatures for one sampling

date, and convergence of possible model results for three isotopic signatures. We are not able to separate these uncertainties in this study.

Another measure of model performance is given by the correlations between obtained results of all the modeled probable solutions (Fig. S4). Previous studies applying similar models interpreted the strong negative correlations between determined mixing proportions as inability of the model to distinguish these sources (Moore and Semmens, 2008; Parnell et al., 2013; Phillips et al., 2014). We observe strong negative correlations between f_{bD} and f_{nD} for most cases. This may indicate the uncertainty in determination of these fractions due to the lack of isotopic separation of these processes in the $\delta^{15}\text{N}^{\text{sp}}/\delta^{18}\text{O}$ space (Fig. 1). But such a correlation is also expected if we deal with two strongly dominating sources, and the correlations between f_{bD} and f_{nD} are indeed highest for F3, where the fractions of other pathways are lowest. Nevertheless, for fractions showing high correlations, presentation of the sum of these both pathways may be much more informative than separation between them. Therefore, we observe much more stable results for the sum of f_{bD} and f_{nD} than for f_{bD} alone (Fig. 7). However, the large variations of f_{bD} are not only the modeling artifact, since they reflect the variations noted with the reference method, which is especially clear for F3 (see Fig. 7E). In this case study, we can see that the variations of f_{bD} are larger than in the reference method but similar dynamics of these variations can be observed. With the model we can quantify the contribution of four pathways, however, there are so far no precise enough reference methods to validate these results (Wrage-Mönnig et al., 2018) (see Section 3.10). But are the provided estimates plausible? We can check with the most characteristic outcomes. For F1 the highest f_{fD} values were noted (Fig. 4). For this field study also the highest $r_{\text{N}_2\text{O}}$ and the lowest f_{bD} were noted by all the approaches (Table 3, Table 4, Fig. 5C, Fig. 7C). Since for fD N_2O is mostly the final product not further reduced to N_2 (Sutka et al., 2008), the higher f_{fD} should result in higher $r_{\text{N}_2\text{O}}$ values, which was noted for F1. The highest f_{Ni} was noted for F2. In this field study, the soil ammonium content is clearly the highest and nitrate the lowest (Table 2), which indicates that nitrification can be more active here during the whole study campaign, when compared to the other experiments, where we deal with large ammonium consumption at the very beginning of the experiments. This accordance of results allows us to suppose that the general trends in pathways mixing proportions provided by the model is plausible.

4.3 Agreement in estimates of isotopocule approaches and independent estimates

In general, the both cases of SP/O Map and Case 2 of 3DI model show very similar results, whereas Case 1 of 3DI model indicates always higher $r_{\text{N}_2\text{O}}$ values, hence underestimates N_2 flux (Table 3, Fig. 5). For the SP/O Map, the application of different calculation cases has little impact on the final results because both cases show very high and quite stable f_{bD} . The contribution of bD is expressed jointly with nD for the SP/O Map, due to their isotopic overlap (see Section 3.5). As a result, the necessary assumption for the SP/O Map is the possible reduction of N_2O originating from these both fractions bD and nD, also for Case 1. Conversely for 3DI model,

these both fractions are separated and for Case 1 only bD fraction can be reduced. The r_{bD} values obtained for Case 1 are very low (eg. 0.2 for F2 and 0.15 for F3) but when recalculated to r_{N_2O} (for comparison with other results) they get high (eg. 0.58 for F2 and 0.54 for F3, Table 3) due to respective f_{bD} values (see Eq. 15).

Therefore, the r_{N_2O} determined by 3DI model Case 1 is very vulnerable to proper determination of f_{bD} . And this fraction is not very precisely determined, as we know from strong correlation found for f_{bD} / f_{nD} (see Section 4.2). Consequently, the imprecise separation of f_{bD} and f_{nD} is the reason for the biased r_{N_2O} values for Case 1 3DI model. This bias is not significant when we deal with very high r_{N_2O} fraction, as for F1 (Table 3) or for very high and stable bD contribution, as for L2 (Table 3, Fig. 7B). For Case 2 the lack of precision in f_{bD} and f_{nD} determination do not largely affect r_{N_2O} results, since N_2O originating from all pathways can be reduced in this case (Eq.14). Hence, in further discussion for 3DI model results we take into account Case 2 outputs only. This observation may also indicate that not only N_2O from heterotrophic bacterial denitrification can be further reduced to N_2 . Although previous studies suggested rather the Case 1 to be more accurate (Verhoeven et al., 2019; Wu et al., 2019), our comparison indicates that Case 1 of the 3DI model underestimates the N_2O reduction in most cases (Table 3). This may reinforce a recent discussion on nitrifier denitrification mechanisms assuming that heterotrophic bacterial denitrifiers are relevant in reducing NO_2^- from nitrification (Hink et al., 2017). This would support the assumption that N_2O from nD can be further reduced by bD pathway.

The largest discrepancy in r_{N_2O} between isotopocule approaches and reference method is noted for F2 (Table 3). In this field campaign we deal with very low N_2O fluxes and the reference method indicates very low r_{N_2O} values, i.e., very high N_2O reduction rate. Moreover, for F2 the highest soil moisture of the field studies was noted (Table 2), which may result in inhibition of gaseous exchange. In these conditions, it is very probable that some of the produced N_2O is completely reduced, and consequently, the isotopic information on its reduction is missed. Complete N_2O reduction in soil microsites would result in overestimation of r_{N_2O} values by the N_2O isotopocule approaches and this is what we observe in this case (Fig. 5D).

Pronounced discrepancies in mean values are also noted for L2 laboratory incubation (Table 3), which is due to rapid changes in r_{N_2O} resulting from water addition (Fig. 5B, Section 4.1). This rapid change is noted in both SP/O Map and 3DI model and in the reference method, but the N_2O isotopocule results seem to react slower and with lower amplitude. N_2O isotopocule approaches base on isotopic analyses of N_2O , whereas ^{15}N gas-flux method base on the direct N_2 measurements. If N_2O is partially stored in soil we may deal with delay in our observations or discrepancy in results. This indicates that individual sudden changes are not well monitored by the isotopocule approaches but the general mean values and changing trends are very well reflected (Table 3, Fig. 6).

Summary statistics for agreement between isotopocule approaches and reference method indicate significant fit for SP/O Map, where both cases show very similar fit, and for 3DI model Case 2, where the best fit was observed (Table 3). This agreement is much better than recently shown by Wu et al. (2019), where numerous

cases with very poor agreement between the results of O/SP Map and reference method have been found. That study analyzed archival datasets, from which many experiments consisted of various experimental phases – like anoxic and oxic or before and after fertilizer addition. This might have complicated the comparability of the results. As shown by our study, the sudden changes in experimental conditions are differently reflected in the results of both methods. Whereas the reference method based on direct measurements of N_2 flux reacts immediately, results of isotopocule approaches show a certain delay, possibly due to accumulation of N_2O in the soil (Fig. 5B). But when we compare the mean values for each experimental phase, the agreement between both methods is much better (Fig.6). Additionally, the former study included some experiments with glucose amendment (Wu et al., 2019), which results in a very rapid N turnover and in consequence unstable pathways contribution.

The source partitioning of N_2O production seems much more problematic than of r_{N_2O} values. This is also more difficult to be evaluated with the reference method since it yields only the sum of fD and bD, *i.e.*, it does not distinguish these individual processes (see Section 3.10). We are also aware that the model may not be very precise in separation of f_{bD} , f_{nD} and f_{fD} , since they often show strong negative correlation (see Section 3.8 and 4.2). Taking these considerations into account, we can well understand the fractions contribution for L1, L2 and F3, where the f_{bD} fraction of SP/O Map and f_{bD+nD} of 3DI model are comparable and f_{bD+fD} of the 3DI model and $f_{P_N_2O}$ of the ^{15}N gas-flux method show similar range and trends (Fig. 7A, 7B, 7E). However, a large bias in source partition is observed for F1 and F2 field studies. The $f_{P_N_2O}$ determined by ^{15}N gas-flux method is much lower than any fraction determined with isotopocule methods (Fig. 7C, 7D). The very low $f_{P_N_2O}$ fraction indicates large contribution of N_2O originating from unlabelled pool, since the $f_{P_N_2O}$ of the labeled $^{15}NH_4^+$ treatment was also comparably low (data not shown). This N_2O may originate from organic N pool pathway (Müller et al., 2014; Zhang et al., 2015) or chemodenitrification (Wei et al., 2019). These processes are not included in the isotopocule methods hence cannot be accounted for. For these two field studies F1 and F2 we deal with relatively low fluxes and low temperatures, thus the processes invisible for high flux situations may play significant role here.

4.4 Possible origins of inconsistency and potential improvements

From the comparison of isotopocule approaches and the reference method we can identify the condition when the calculation based on natural abundance N_2O isotopes may be biased. The Maps applying $\delta^{15}N$ value are very vulnerable to changes in substrate isotopic signatures. When we observe large variations in soil NO_3^- , NO_2^- or NH_4^+ isotopic signatures such approach should rather not be applied.

Most problematic is the occurrence of N_2O production pathways which are so far not investigated for their characteristic isotopic signature. This might be heterotrophic nitrification, co-denitrification or chemodenitrification, as supposed for our case studies F1 and F2. These less examined processes gain on

significance when the N₂O fluxes are generally low, like in F1 and F2, where N₂O flux was mostly below 10 gN-N₂O ha⁻¹d⁻¹. Hence, for such low N₂O fluxes application of isotope Maps and 3DI model may be less precise.

Recent literature suggest that the most vulnerable value for SP/O Map is the isotopic signature of the bD mixing endmember and this parameter should be best determined in focused experiments (Buchen et al., 2018; Wu et al., 2019). It was shown that a short-term anoxic experiment with N₂O reduction inhibition with C₂H₂ favors bD (Lewicka-Szczebak et al., 2017; Lewicka-Szczebak et al., 2016). Such an experiment could have been used for determination of isotopic signature of bacterial denitrification characteristic for the particular soil used in this study and narrow the range of mixing endmember for bD pathway. Unfortunately, when planning and conducting these studies we did not have this complete knowledge and missed to perform such parallel anoxic incubations, but this should be strongly recommended for further studies applying SP/O Map or 3DI model.

The determination of initial delta values (δ_0), unchanged by N₂O reduction might be also helpful in further constraining the isotope Maps. These δ_0 can be obtained from the relation of r_{N_2O} determined by reference method and measured isotopic signatures (Lewicka-Szczebak et al., 2017). Unfortunately, this approach was not successful for our data, because no significant correlation between r_{N_2O} and isotopic signatures could be found. This indicates unstable endmembers mixing proportions or some problems with parallel experiments. This was also the case in previous validation experimental study (Lewicka-Szczebak et al., 2017), where for oxic conditions the variations were too high to obtain significant correlation and determine the δ_0 values. This shows that oxic experiments are not well suited for determination of isotopic signatures of particular mixing endmembers and should be always accompanied by more focused and stable anoxic incubations.

Further enhancement in performance of the isotope Maps could be attained if the experiments determining the initial isotopic composition of mixing endmembers were performed with the soil collected parallel to particular experiments and the anoxic incubations were performed in the conditions similar to field conditions during the particular case study. Possibly from such experiments some subtle differences in characteristic endmember isotopic signatures would be detected. It can be supposed that such differences could be the reason for worse r_{N_2O} agreement with reference method for L2 and F2 (Table 3). It has been shown that the changes in initial $\delta^{18}O$ value of bacterial denitrification endmember has significant impact on the final results (Wu et al., 2019). We have checked if this could bring better agreement. For L2 the perfect agreement of SP/O Map and reference method is obtained when applying slightly higher $\delta^{18}O$ values: 25 ‰ instead of 19 ‰. Conversely for F2, much lower $\delta^{18}O$ values: 10 ‰ instead of 19 ‰ would be needed to obtain the perfect agreement. This differences are quite possible, the low values for F2 might be a result of low temperature and low fluxes, and in consequence moderate or slow processes associated with maximal O-exchange. On the contrary, for high water content and high temperature in L2 experiment we can expect slightly lower O-exchange resulting in higher initial $\delta^{18}O$ values.

Conclusions

- It was shown that N_2O residual fraction can be calculated based on isotope fractionation during N_2O reduction with SP/O Map. The SP/N Map appeared more complex and problematic.
- Here we present for the first time the idea of applying a model based on three N_2O isotopic signatures. We are convinced that this is a powerful step forward in development of N_2O isotopocule methods to quantify especially $r_{\text{N}_2\text{O}}$, but also estimate some mixing proportions of the four N_2O pathways included in the model.
- Both N_2O isotopocule based approaches - SP/O Map and 3DI model (Case 2) – show good accordance of $r_{\text{N}_2\text{O}}$ with reference method and very comparable results to each other. For 3DI model the results of Case 1 (assuming N_2O reduction of bacterial denitrification only) underestimate the N_2 flux due to imprecision in determination of f_{bD} .
- The determination of mixing proportions with N_2O isotopocule based approaches is biased for cases where additional processes not incorporated into the model occur. This may be the case when very low N_2O fluxes are noted.
- N_2 flux determined from ^{15}N labelled treatments (reference method) show more rapid changes compared to values determined with N_2O isotopocule approaches. Hence, the $r_{\text{N}_2\text{O}}$ determined with N_2O isotopocule approaches provides a good approximation of the averaged N_2O reduction range, but do not reflect dynamic changes of $r_{\text{N}_2\text{O}}$ with high resolution.
- 3DI model allows for a good control of the results quality, which is a clear advantage over the results provided with SP/O Map.
- According to these findings, the SP/O Map and 3DI model can be applied for $r_{\text{N}_2\text{O}}$ determination with expected precision of around 0.15. For cases where the mixing proportions separation is imprecise, which can be supposed when model results show high negative correlations, the results should be carefully interpreted and preferably the values of correlated fractions should be shown jointly. In such cases, the calculation Case 2 should be applied for $r_{\text{N}_2\text{O}}$ determination, since Case 1 incorporates possibly biased f_{bD} into the final $r_{\text{N}_2\text{O}}$ value. Importantly, even for these cases where the determination of mixing proportions was biased, we got reasonable estimates of $r_{\text{N}_2\text{O}}$ values (with Case 2 calculations).

Data availability. Original data are available upon request. Material necessary for this study findings is presented in the paper and supplementary materials.

Author contribution. DLS and RW designed the field studies and laboratory experiments and DLS was in charge of caring them out. DLS performed the interpretations based on isotope mapping approaches and initiated

the idea of three-dimensional model. MPL developed the model and provided results for analysed case studies with graphical presentations. DLS prepared the manuscript with significant contribution of RW and MPL.

Competing interests. The authors declare that they have no conflict of interest.

930

Acknowledgements. This study was financed by German Research Foundation (grant LE 3367/1-1 to DLS) and conducted in cooperation with the research unit 2337: “Denitrification in Agricultural Soils: Integrated Control and Modeling at Various Scales (DASIM)” (German Research Foundation, grant WE 1904/10-1 to RW). Many thanks are due to Frank Hegewald and Nicolas Ruoss for help in conducting field studies, Stefan Burkart for help in carrying out soil incubation, Martina Heuer for help in isotopic analyses, Nicole Altwein and Ute Tambor for help in preparing laboratory incubation and in soil analyses, Kerstin Gilke for chromatographic analyses and Caroline Buchen for advice in preparing field campaigns.

935

References:

- Aulakh, M. S., Doran, J. W., and Mosier, A. R.: Field-Evaluation of 4 Methods for Measuring Denitrification, *Soil Sci Soc Am J*, 55, 1332-1338, 1991.
- Baily, A., Watson, C. J., Laughlin, R., Matthews, D., McGeough, K., and Jordan, P.: Use of the ^{15}N gas flux method to measure the source and level of N_2O and N_2 emissions from grazed grassland, *Nutr Cycl Agroecosys*, 94, 287-298, 2012.
- Barford, C. C., Montoya, J. P., Altabet, M. A., and Mitchell, R.: Steady-state nitrogen isotope effects of N_2 and N_2O production in *Paracoccus denitrificans*, *Appl Environ Microb*, 65, 989-994, 1999.
- Baumgärtel, B. and Benke, M.: Düngeempfehlungen Stickstoff: Getreide, Raps, Hackfrüchte., Landwirtschaftskammer Niedersachsen - Geschäftsbereich Landwirtschaft, 2009. 2009.
- Bergsma, T. T., Ostrom, N. E., Emmons, M., and Robertson, G. P.: Measuring simultaneous fluxes from soil of N_2O and N_2 in the field using the ^{15}N -Gas "nonequilibrium" technique, *Environ Sci Technol*, 35, 4307-4312, 2001.
- Bergstermann, A., Cardenas, L., Bol, R., Gilliam, L., Goulding, K., Meijide, A., Scholefield, D., Vallejo, A., and Well, R.: Effect of antecedent soil moisture conditions on emissions and isotopologue distribution of N_2O during denitrification, *Soil Biol Biochem*, 43, 240-250, 2011.
- Böhlke, J. K., Smith, R. L., and Hannon, J. E.: Isotopic analysis of N and O in nitrite and nitrate by sequential selective bacterial reduction to N_2O , *Anal Chem*, 79, 5888-5895, 2007.
- Bouwman, A. F., Beusen, A. H. W., Griffioen, J., Van Groenigen, J. W., Hefting, M. M., Oenema, O., Van Puijenbroek, P. J. T. M., Seitzinger, S., Slomp, C. P., and Stehfest, E.: Global trends and uncertainties in terrestrial denitrification and N_2O emissions, *Philos T R Soc B*, 368, 2013.
- Brenninkmeijer, C. A. M. and Röckmann, T.: Mass spectrometry of the intramolecular nitrogen isotope distribution of environmental nitrous oxide using fragment-ion analysis, *Rapid Commun Mass Sp*, 13, 2028-2033, 1999.
- Buchen, C., Lewicka-Szczebak, D., Fuß, R., Helfrich, M., Flessa, H., and Well, R.: Fluxes of N_2 and N_2O and contributing processes in summer after grassland renewal and grassland conversion to maize cropping on a Plaggic Anthrosol and a Histic Gleysol, *Soil Biol Biochem*, 101, 6-19, 2016.

- 965 Buchen, C., Lewicka-Szczebak, D., Flessa, H., and Well, R.: Estimating N₂O processes during grassland renewal and grassland conversion to maize cropping using N₂O isotopocules, *Rapid Commun Mass Sp*, 32 (13), 1053-1067, 2018.
- Butterbach-Bahl, K., Baggs, E. M., Dannenmann, M., Kiese, R., and Zechmeister-Boltenstern, S.: Nitrous oxide emissions from soils: how well do we understand the processes and their controls?, *Philos T R Soc B*, 368, 2013.
- 970 Cardenas, L., Bol, R., D., L.-S., Gregory, A. S., Matthews, G. P., Whalley, W. R., Misselbrook, R., Scholefield, D., and Well, R.: Effect of soil saturation on denitrification in a grassland soil, *Biogeosciences*, 14, 4691-4710, 2017.
- Casciotti, K. L., Sigman, D. M., Hastings, M. G., Bohlke, J. K., and Hilkert, A.: Measurement of the oxygen isotopic composition of nitrate in seawater and freshwater using the denitrifier method, *Anal Chem*, 74, 4905-4912, 2002.
- 975 Castellano-Hinojosa, A., Loick, N., Dixon, E., Matthews, G. P., Lewicka-Szczebak, D., Well, R., Bol, R., Charteris, A., and Cardenas, L.: Improved isotopic model based on ¹⁵N tracing and Rayleigh-type isotope fractionation for simulating differential sources of N₂O emissions in a clay grassland soil, *Rapid Communication in Mass Spectrometry*, 33, 449-460, 2019.
- 980 Decock, C. and Six, J.: An assessment of N-cycling and sources of N₂O during a simulated rain event using natural abundance ¹⁵N, *Agr Ecosyst Environ*, 165, 141-150, 2013.
- Eschenbach, W., Lewicka-Szczebak, D., Stange, C. F., Dyckmans, J., and Well, R.: Measuring ¹⁵N Abundance and Concentration of Aqueous Nitrate, Nitrite, and Ammonium by Membrane Inlet
- 985 Quadrupole Mass Spectrometry, *Anal Chem*, 89, 6076-6081, 2017.
- Felix, J. D., Elliott, E. M., Gish, T. J., McConnell, L. L., and Shaw, S. L.: Characterizing the isotopic composition of atmospheric ammonia emission sources using passive samplers and a combined oxidation-bacterial denitrifier approach, *Rapid Communication in Mass Spectrometry*, 27, 2239–2246, 2013.
- 990 Firestone, M. K. and Davidson, E. A.: Microbial basis of NO and N₂O production and consumption in soil. In: *Exchange of trace gases between terrestrial ecosystems and the atmosphere.*, Andreae, M. O. and Schimel, D. S. (Eds.), John Wiley and Sons, New York, 1989.
- Frame, C. H. and Casciotti, K. L.: Biogeochemical controls and isotopic signatures of nitrous oxide production by a marine ammonia-oxidizing bacterium, *Biogeosciences*, 7, 2695-2709, 2010.
- 995 Fuß, R., last access: 10.01.2020, 2015.
- Groffman, P. M.: Terrestrial denitrification: challenges and opportunities, *Ecological Processes*, 2012, 1-11, 2012.
- Groffman, P. M., Altabet, M. A., Bohlke, J. K., Butterbach-Bahl, K., David, M. B., Firestone, M. K., Giblin, A. E., Kana, T. M., Nielsen, L. P., and Voytek, M. A.: Methods for measuring denitrification: Diverse approaches to a difficult problem, *Ecol Appl*, 16, 2091-2122, 2006.
- 1000 Hink, L., Lycus, P., Gubry-Rangin, C., Frostegård, A., Nicol, G. W., Prosser, J. I., and Bakken, L. R.: Kinetics of NH₃⁺ oxidation, NO⁻ turnover, N₂O⁻ production and electron flow during oxygen depletion in model bacterial and archaeal ammonia oxidisers, *Environ Microbiol*, 19, 4882-4896, 2017.
- Ibraim, E., Wolf, B., Harris, E., Gasche, R., Wei, J., Longfei, Y., Kiese, R., Eggleston, S., Butterbach-Bahl, K., Zeeman, M., Tuzson, B., Emmenegger, L., Six, J., Henne, S., and Mohn, J.: Attribution of N₂O sources in a grassland soil with laser spectroscopy based isotopocule analysis, *Biogeosciences*, 16, 3247–3266, 2019.
- 1005

- IPCC: Climate Change 2007: The Physical Science Basis. Contribution of Working Group I to the Fourth Assessment Report of the Intergovernmental Panel on Climate Change, 2007.
- 1010 Jinuntuya-Nortman, M., Sutka, R. L., Ostrom, P. H., Gandhi, H., and Ostrom, N. E.: Isotopologue fractionation during microbial reduction of N_2O within soil mesocosms as a function of water-filled pore space, *Soil Biol Biochem*, 40, 2273-2280, 2008.
- Kato, T., Toyoda, S., Yoshida, N., Tang, Y. H., and Wada, E.: Isotopomer and isotopologue signatures of N_2O produced in alpine ecosystems on the Qinghai-Tibetan Plateau, *Rapid Commun Mass Sp*, 27, 1517-1526, 2013.
- 1015 Knowles, R.: Denitrification, *Microbiol Rev*, 46, 43-70, 1982.
- Koba, K., Osaka, K., Tobari, Y., Toyoda, S., Ohte, N., Katsuyama, M., Suzuki, N., Itoh, M., Yamagishi, H., Kawasaki, M., Kim, S. J., Yoshida, N., and Nakajimag, T.: Biogeochemistry of nitrous oxide in groundwater in a forested ecosystem elucidated by nitrous oxide isotopomer measurements, *Geochimica et Cosmochimica Acta*, 73, 3115-3133, 2009.
- 1020 Kool, D. M., Wrage, N., Oenema, O., Dolfing, J., and Van Groenigen, J. W.: Oxygen exchange between (de) nitrification intermediates and H_2O and its implications for source determination of NO_3^- and N_2O : a review, *Rapid Commun Mass Sp*, 21, 3569-3578, 2007.
- Kool, D. M., Wrage, N., Oenema, O., Harris, D., and Van Groenigen, J. W.: The ^{18}O signature of biogenic nitrous oxide is determined by O exchange with water, *Rapid Commun Mass Sp*, 23, 104-108, 2009.
- 1025 Kramps-Alpmann, D., Ruoss, N., Korte K., Ernst, U., and Schäfer, B. C.: Klimaoptimierte Anpassungsstrategien in der Landwirtschaft (optimierter Klimabetrieb) II., Unpublished project report, 2017. 2017.
- 1030 Kulkarni, M. V., Burgin, A. J., Groffman, P. M., and Yavitt, J. B.: Direct flux and ^{15}N tracer methods for measuring denitrification in forest soils, *Biogeochemistry*, 117, 359-373, 2013.
- Lewicka-Szczebak, D., Augustin, J., Giesemann, A., and Well, R.: Quantifying N_2O reduction to N_2 based on N_2O isotopocules - validation with independent methods (helium incubation and ^{15}N gas flux method). , *Biogeosciences*, 14, 711-732, 2017.
- 1035 Lewicka-Szczebak, D., Dyckmanns, J., Kaiser, J., Marca, A., Augustin, J., and Well, R.: Oxygen isotope fractionation during N_2O production by soil denitrification, *Biogeosciences*, 13, 1129-1144, 2016.
- Lewicka-Szczebak, D. and Well, R.: The ^{15}N gas-flux method to determine N_2 flux : a comparison of different tracer addition approaches, *SOIL*, 6, 145-152, 2020.
- Lewicka-Szczebak, D., Well, R., Bol, R., Gregory, A., Matthews, P., Misselbrook, T., Whalley, R., and Cardenas, L.: Isotope fractionation factors controlling isotopocule signatures of soil-emitted N_2O produced by denitrification processes of various rates, *Rapid Commun Mass Sp*, 29, 269-282, 2015.
- 1040 Lewicka-Szczebak, D., Well, R., Giesemann, A., Rohe, L., and Wolf, U.: An enhanced technique for automated determination of ^{15}N signatures of N_2 , ($\text{N}_2+\text{N}_2\text{O}$) and N_2O in gas samples, *Rapid Commun Mass Sp*, 27, 1548-1558, 2013.
- 1045 Lewicka-Szczebak, D., Well, R., Koster, J. R., Fuss, R., Senbayram, M., Dittert, K., and Flessa, H.: Experimental determinations of isotopic fractionation factors associated with N_2O production and reduction during denitrification in soils, *Geochim Cosmochim Ac*, 134, 55-73, 2014.
- Maeda, K., Spor, A., Edel-Hermann, V., Heraud, C., Breuil, M. C., Bizouard, F., Toyoda, S., Yoshida, N., Steinberg, C., and Philippot, L.: N_2O production, a widespread trait in fungi, *Sci Rep-Uk*, 5, 9697: 9691-9697, 2015.
- 1050

- Mandernack, K. W., Mills, C. T., Johnson, C. A., Rahn, T., and Kinney, C.: The $\delta^{15}\text{N}$ and $\delta^{18}\text{O}$ values of N_2O produced during the co-oxidation of ammonia by methanotrophic bacteria, *Chem Geol*, 267, 96-107, 2009.
- Mathieu, O., Leveque, J., Henault, C., Milloux, M. J., Bizouard, F., and Andreux, F.: Emissions and spatial variability of N_2O , N_2 and nitrous oxide mole fraction at the field scale, revealed with ^{15}N isotopic techniques, *Soil Biol Biochem*, 38, 941-951, 2006.
- Menyailo, O. V. and Hungate, B. A.: Stable isotope discrimination during soil denitrification: Production and consumption of nitrous oxide, *Global Biogeochem Cy*, 20, GB3025, 2006.
- Moore, J. W. and Semmens, B. X.: Incorporating uncertainty and prior information into stable isotope mixing models, *Ecology Letters*, 11, 470-480, 2008.
- Morse, J. L. and Bernhardt, E. S.: Using ^{15}N tracers to estimate N_2O and N_2 emissions from nitrification and denitrification in coastal plain wetlands under contrasting land-uses, *Soil Biol Biochem*, 57, 635-643, 2013.
- Mosier, A. R., Guenzi, W. D., and Schweizer, E. E.: Field Denitrification Estimation by N-15 and Acetylene Inhibition Techniques, *Soil Sci Soc Am J*, 50, 831-833, 1986.
- Müller, C., Laughlin, R. J., Spott, O., and Rütting, T.: Quantification of N_2O emission pathways via a ^{15}N tracing model, *Soil Biol Biochem*, 72, 44-54, 2014.
- Nash, J. E. and Sutcliffe, J. V.: River flow forecasting through conceptual models part I— a discussion of principles. , *J Hydrol*, 10, 282-290, 1970.
- Opdyke, M. R., Ostrom, N. E., and Ostrom, P. H.: Evidence for the predominance of denitrification as a source of N_2O in temperate agricultural soils based on isotopologue measurements, *Global Biogeochem Cy*, 23, GB4018: 4011-4010, 2009.
- Ostrom, N. E., Pitt, A., Sutka, R., Ostrom, P. H., Grandy, A. S., Huizinga, K. M., and Robertson, G. P.: Isotopologue effects during N_2O reduction in soils and in pure cultures of denitrifiers, *J Geophys Res-Bioge*, 112, G02005: 02001-02012, 2007.
- Ostrom, N. E., Sutka, R., Ostrom, P. H., Grandy, A. S., Huizinga, K. M., Gandhi, H., von Fischer, J. C., and Robertson, G. P.: Isotopologue data reveal bacterial denitrification as the primary source of N_2O during a high flux event following cultivation of a native temperate grassland, *Soil Biol Biochem*, 42, 499-506, 2010.
- Park, S., Perez, T., Boering, K. A., Trumbore, S. E., Gil, J., Marquina, S., and Tyler, S. C.: Can N_2O stable isotopes and isotopomers be useful tools to characterize sources and microbial pathways of N_2O production and consumption in tropical soils?, *Global Biogeochem Cy*, 25, GB1001, 2011.
- Parnell, A. C., Phillips, D. L., Bearhop, S., Semmens, B. X., Ward, E. J., Moore, J. W., Jackson, A. L., Grey, J., Kelly, D. J., and Inger, R.: Bayesian stable isotope mixing models, *Environmetrics*, 24, 387-399, 2013.
- Phillips, D. L., Inger, R., Bearhop, S., Jackson, A. L., Moore, J. W., Parnell, A. C., Semmens, B. X., and Ward, E. J.: Best practices for use of stable isotope mixing models in food-web studies, *Canadian Journal of Zoology* 92, 823–835, 2014.
- Ravishankara, A. R., Daniel, J. S., and Portmann, R. W.: Nitrous Oxide (N_2O): The Dominant Ozone-Depleting Substance Emitted in the 21st Century, *Science*, 326, 123-125, 2009.
- Röckmann, T., Kaiser, J., Brenninkmeijer, C. A. M., and Brand, W. A.: Gas chromatography/isotope-ratio mass spectrometry method for high-precision position-dependent ^{15}N and ^{18}O measurements of atmospheric nitrous oxide, *Rapid Commun Mass Sp*, 17, 1897-1908, 2003.

- Rohe, L., Anderson, T.-H., Braker, G., Flessa, H., Giesemann, A., Lewicka-Szczebak, D., Wrage-Mönnig, N., and Well, R.: Dual isotope and isotopomer signatures of nitrous oxide from fungal denitrification – a pure culture study, *Rapid Commun Mass Sp*, 28, 1893-1903, 2014a.
- Rohe, L., Anderson, T. H., Braker, G., Flessa, H., Giesemann, A., Wrage-Mönnig, N., and Well, R.: Fungal oxygen exchange between denitrification intermediates and water, *Rapid Commun Mass Sp*, 28, 377-384, 2014b.
- Rohe, L., Well, R., and Lewicka-Szczebak, D.: Use of oxygen isotopes to differentiate between nitrous oxide produced by fungi or bacteria during denitrification, *Rapid Communication in Mass Spectrometry*, 31, 1297-1312, 2017.
- Saggar, S., Jha, N., Deslippe, J., Bolan, S., Luo, J., Giltrap, D. L., Kim, D.-G., Zaman, M., and Tillman, R. W.: Denitrification and $N_2O:N_2$ production in temperate grasslands: Processes, measurements, modelling and mitigating negative impacts, *Science of the Total Environment*, 465, 173-195, 2013.
- Schmidt, G., Segschneider H.-J., and R., R.: Bestimmung der ^{15}N Häufigkeit bei nichtstatistischer ^{15}N -verteilung in N_2 sowie bei N_2O in Bodenluftproben mittels GC-R-IRMS-Kopplung in einem Probenlauf, *Isot Environ Healt S*, 34, 235-243, 1998.
- Scholefield, D., Hawkins, J. M. B., and Jackson, S. M.: Development of a helium atmosphere soil incubation technique for direct measurement of nitrous oxide and dinitrogen fluxes during denitrification, *Soil Biol Biochem*, 29, 1345-1352, 1997.
- Seitzinger, S.: Nitrogen cycle - Out of reach, *Nature*, 452, 162-163, 2008.
- Senbayram, M., Chen, R., Budai, A., Bakken, L., and Dittert, K.: N_2O emission and the $N_2O/(N_2O + N_2)$ product ratio of denitrification as controlled by available carbon substrates and nitrate concentrations, *Agr Ecosyst Environ*, 147, 4-12, 2012.
- Sigman, D. M., Casciotti, K. L., Andreani, M., Barford, C., Galanter, M., and Bohlke, J. K.: A bacterial method for the nitrogen isotopic analysis of nitrate in seawater and freshwater, *Anal Chem*, 73, 4145-4153, 2001.
- Spott, O., Russow, R., Apelt, B., and Stange, C. F.: A N -15-aided artificial atmosphere gas flow technique for online determination of soil N_2 release using the zeolite Kostrolith SX6 (R), *Rapid Commun Mass Sp*, 20, 3267-3274, 2006.
- Stange, C. F., Spott, O., Apelt, B., and Russow, R. W. B.: Automated and rapid online determination of ^{15}N abundance and concentration of ammonium, nitrite, or nitrate in aqueous samples by the SPINMAS technique, *Isot Environ Healt S*, 43, 227-236, 2007.
- Stevens, R. J. and Laughlin, R. J.: Nitrite Transformations during Soil Extraction with Potassium-Chloride, *Soil Sci Soc Am J*, 59, 933-938, 1995.
- Sutka, R. L., Adams, G. C., Ostrom, N. E., and Ostrom, P. H.: Isotopologue fractionation during N_2O production by fungal denitrification, *Rapid Commun Mass Sp*, 22, 3989-3996, 2008.
- Sutka, R. L., Ostrom, N. E., Ostrom, P. H., Breznak, J. A., Gandhi, H., Pitt, A. J., and Li, F.: Distinguishing nitrous oxide production from nitrification and denitrification on the basis of isotopomer abundances, *Appl Environ Microb*, 72, 638-644, 2006.
- Toyoda, S., Mutoke, H., Yamagishi, H., Yoshida, N., and Tanji, Y.: Fractionation of N_2O isotopomers during production by denitrifier, *Soil Biol Biochem*, 37, 1535-1545, 2005.
- Toyoda, S., Yano, M., Nishimura, S., Akiyama, H., Hayakawa, A., Koba, K., Sudo, S., Yagi, K., Makabe, A., Tobari, Y., Ogawa, N. O., Ohkouchi, N., Yamada, K., and Yoshida, N.: Characterization and

- production and consumption processes of N₂O emitted from temperate agricultural soils determined via isotopomer ratio analysis, *Global Biogeochem Cy*, 25, GB2008, 2011.
- Toyoda, S. and Yoshida, N.: Determination of nitrogen isotopomers of nitrous oxide on a modified isotope ratio mass spectrometer, *Anal Chem*, 71, 4711-4718, 1999.
- 1140 Toyoda, S., Yoshida, N., and Koba, K.: Isotopocule analysis of biologically produced nitrous oxide in various environments, *Mass Spectrometry Reviews*, doi: 10.1002/mas.21459, 2017. 2017.
- Verhoeven, E., Barthel, M., Yu, L., Celi, L., Said-Pullicino, D., Sleutel, S., Lewicka-Szczebak, D., Six, J., and Decock, C.: Early season N₂O emissions under variable water management in rice systems: source-partitioning emissions using isotope ratios along a depth profile, *Biogeosciences*, 16 (2), 383-408, 2019.
- 1145 Wei, J., Ibraim, E., Brüggemann, N., Vereecken, H., and Mohn, J.: First real-time isotopic characterisation of N₂O from chemodenitrification, *Geochim Cosmochim Acta*, 267, 17-32, 2019.
- Well, R., Burkart, S., Giesemann, A., Grosz, B., Köster, J. R., and Lewicka-Szczebak, D.: Improvement of the ¹⁵N gas flux method for in situ measurement of soil denitrification and its product stoichiometry, *Rapid Commun Mass Sp*, 33, 437-448, 2019a.
- 1150 Well, R., Eschenbach, W., Flessa, H., von der Heide, C., and Weymann, D.: Are dual isotope and isotopomer ratios of N₂O useful indicators for N₂O turnover during denitrification in nitrate-contaminated aquifers?, *Geochim Cosmochim Acta*, 90, 265-282, 2012.
- Well, R. and Flessa, H.: Isotope fractionation factors of N₂O diffusion, *Rapid Commun Mass Sp*, 22, 2621-2628, 2008.
- 1155 Well, R. and Flessa, H.: Isotopologue enrichment factors of N₂O reduction in soils, *Rapid Commun Mass Sp*, 23, 2996-3002, 2009.
- Well, R., Maier, M., Lewicka-Szczebak, D., Köster, J. R., and Ruoss, N.: Underestimation of denitrification rates from field application of the ¹⁵N gas flux method and its correction by gas diffusion modelling, *Biogeosciences*, 16, 2233-2246, 2019b.
- 1160 Westley, M. B., Popp, B. N., and Rust, T. M.: The calibration of the intramolecular nitrogen isotope distribution in nitrous oxide measured by isotope ratio mass spectrometry, *Rapid Commun Mass Sp*, 21, 391-405, 2007.
- Wolf, B., Merbold, L., Decock, C., Tuzson, B., Harris, E., Six, J., Emmenegger, L., and Mohn, J.: First on-line isotopic characterization of N₂O above intensively managed grassland, *Biogeosciences*, 12, 2517-2531, 2015.
- 1165 Wrage-Mönnig, N., Horn, M. A., Well, R., Müller, C., Velthof, G., and Oenema, O.: The role of nitrifier denitrification in the production of nitrous oxide revisited, *Soil Biology and Biochemistry*, 123, A3-A16, 2018.
- 1170 Wu, D., Well, R., Cárdenas, L. M., Fuß, R., Lewicka-Szczebak, D., Köster, J. R., Brüggemann, N., and Bol, R.: Quantifying N₂O reduction to N₂ during denitrification in soils via isotopic mapping approach: Model evaluation and uncertainty analysis, *Environmental Research*, 2019. 108806, 2019.
- Wu, H. H., Dannenmann, M., Fanselow, N., Wolf, B., Yao, Z. S., Wu, X., Brüggemann, N., Zheng, X. H., Han, X. G., Dittert, K., and Butterbach-Bahl, K.: Feedback of grazing on gross rates of N mineralization and inorganic N partitioning in steppe soils of Inner Mongolia, *Plant Soil*, 340, 127-139, 2011.
- 1175 Yamagishi, H., Westley, M. B., Popp, B. N., Toyoda, S., Yoshida, N., Watanabe, S., Koba, K., and Yamanaka, Y.: Role of nitrification and denitrification on the nitrous oxide cycle in the eastern tropical North Pacific and Gulf of California, *J Geophys Res-Biogeophys*, 112, 2007.

- Yoshida, N.: ^{15}N -depleted N_2O as a product of nitrification., *Nature*, 335, 528-529, 1988.
- 1180 Yu, L., Harris, E., Lewicka-Szczebak, D., Barthel, M., Blomberg, M. R. A., Harris, S., Johnson, M. S.,
Lehmann, M. F., Liisberg, J., Müller, C., Ostrom, N., Six, J., Toyoda, S., Yoshida, N., and Mohn, J.: What
can we learn from N_2O isotope data? - Analytics, processes and modelling, *Rapid Communication in
Mass Spectrometry*, 34, e8858, 2020.
- 1185 Zhang, J. B., Muller, C., and Cai, Z. C.: Heterotrophic nitrification of organic N and its contribution to
nitrous oxide emissions in soils, *Soil Biol Biochem*, 84, 199-209, 2015.
- Zhang, L., Altabet, M. A., Wu, T. X., and Hadas, O.: Sensitive measurement of $\text{NH}_4^+ ^{15}\text{N}/^{14}\text{N}$ ($\delta^{15}\text{NH}_4^+$)
at natural abundance levels in fresh and saltwaters, *Anal Chem*, 79, 5297-5303, 2007.
- 1190 Zou, Y., Hirono, Y., Yanai, Y., Hattori, S., Toyoda, S., and Yoshida, N.: Isotopomer analysis of nitrous
oxide accumulated in soil cultivated with tea (*Camellia sinensis*) in Shizuoka, central Japan, *Soil Biol
Biochem*, 77, 276-291, 2014.

Tables and Figures

Table 1: Summary of mixing endmembers isotopic signatures of particular pathways (bD- bacterial denitrification, nD- nitrifier denitrification, fD- fungal denitrification, Ni- nitrification) and reduction fractionation factors (reduction) with respective references. For the model input each value is corrected with the respective mean isotopic signature of the substrate: for $\delta^{18}\text{O}$ – soil water ($\delta^{18}\text{O}_{\text{H}_2\text{O}}$) for bD, nD and fD, for $\delta^{15}\text{N}$ – respective substrate – NO_3^- for bD and fD and NH_4^+ for nD and Ni, with distinct values applied for field ($\delta^{15}\text{N}_{\text{field}}$ for F1, F2, F3) and laboratory ($\delta^{15}\text{N}_{\text{lab}}$ for L1, L2) studies. The respective substrate corrected values were applied as a model input for $\delta^{18}\text{O}$ and $\delta^{15}\text{N}$, for $\delta^{15}\text{N}^{\text{SP}}$ no substrate correction is needed. The final model input values are marked with bold font.

	literature values		substrate isotope values				substrate corrected values		
pathway	$\delta^{15}\text{N}^{\text{SP}}$	$\epsilon^{18}\text{O}$	$\epsilon^{15}\text{N}$	$\delta^{18}\text{O}_{\text{H}_2\text{O}}$	$\delta^{15}\text{N}_{\text{field}}$	$\delta^{15}\text{N}_{\text{lab}}$	$\delta^{18}\text{O}$	$\delta^{15}\text{N}_{\text{field}}$	$\delta^{15}\text{N}_{\text{lab}}$
bD ^a	-1.9±4.6	19.0±2.1	-45.8±4.7	-6.4	11.9	4.5	12.6±2.1	-33.9±4.7	-41.3±4.7
nD ^b	-5.9±6.5	15.7±2.9	-56.9±3.8	-6.4	41.4	79.3	9.3±2.9	-15.5±3.8	22.4±3.8
fD ^c	33.6±2.5	46.9±3.8	-38.0±6.6	-6.4	11.9	4.5	40.5±3.8	-26.1±6.6	-33.5±6.6
Ni ^d	35.0±2.9	23.5±2.1	-57.0±7.3		41.4	79.3		-15.6±7.3	22.3±7.3
reduction ^e	-6.0±1.4	-15.9±4.7	-7.0±2.1						

^a – references for bD (Barford et al., 1999; Lewicka-Szczebak et al., 2016; Lewicka-Szczebak et al., 2014; Rohe et al., 2017; Sutka et al., 2006; Toyoda et al., 2005)

^b – references for nD (Frame and Casciotti, 2010; Sutka et al., 2006)

^c – references for fD (Maeda et al., 2015; Rohe et al., 2014a; Rohe et al., 2017; Sutka et al., 2008)

^d – references for Ni (Frame and Casciotti, 2010; Mandernack et al., 2009; Sutka et al., 2006; Yoshida, 1988)

^e – references for N_2O reduction to N_2 (Jinuntuya-Nortman et al., 2008; Lewicka-Szczebak et al., 2015; Lewicka-Szczebak et al., 2014; Menyailo and Hungate, 2006; Ostrom et al., 2007; Well and Flessa, 2009)

Table 2: Results summary

	treat ment	F1	F2	F3	L1	L2
WFPS [%]		65.1 ±4.3	69.1±4.5	62.4±4.1	60→65	70→80
N ₂ O flux	NA	8.9±7.4	16.3±26.1	331.3±302.9	4.9±4.7	8.5±5.6
[gN-N ₂ O ha ⁻¹ d ⁻¹]	¹⁵ N	5.9±5.5	4.3±3.3	330.9±323.7	1.4±1.0	54.6±50.2
N ₂ flux ^a	¹⁵ N	bd (<11.3)	108.2±84.1 ^b	576.4±285.4	26.6±18.1	45.3±44.5
[gN-N ₂ ha ⁻¹ d ⁻¹]						
r _{N2O} ^a	¹⁵ N	nd (>0.75)	0.06±0.04 ^b	0.33±0.15	0.12±0.10	0.49±0.31
NO ₃ content	NA	13.6±3.1	8.0±2.4	13.6±3.2	21.2±1.5	21.0±1.7
[mg N kg ⁻¹ soil]	¹⁵ N	15.8±6.2	7.5±1.1	15.8±5.5	20.1±0.6	19.4±1.1
NH ₄ content	NA	3.8±2.1	6.4±3.3	3.4±1.5	0.53±0.19	0.71±0.23
[mg N kg ⁻¹ soil]	¹⁵ N	2.0±2.6	5.4±3.1	3.7±1.9	0.58±0.2	0.72±0.15
δ ¹⁵ N _{NO3} [‰]	NA	8.0±5.4	11.7±5.3	12.1±3.7	4.5±0.4	4.7±0.55
δ ¹⁵ N _{NH4} [‰]	NA	31.0 ±8.7	40.5±6.8	42.2±9.1	90.0±7.9	70.4±17.9
a ¹⁵ N _{NO3} [atom %]	¹⁵ N	20.5 ±9.6	40.3±10.1	19.7±5.8	13.6±0.7	13.9±0.8
a ¹⁵ N _{NH4} [atom %]	¹⁵ N	0.7 ±0.6	0.9±0.4	0.5±0.2	0.5±0.03	0.5±0.01
a ¹⁵ N _{NO2} [atom %]	¹⁵ N	15.5 ±9.4	21.9±8.0	10.9±2.3	8.5±6.1	10.3±3.8
δ ¹⁵ N _{N2O}	NA	-33.4 ±9.5	-20.2±16.0	-14.0±14.8	-2.4±8.0	- 17.7±11.9
δ ¹⁸ O _{N2O}	NA	22.7 ±4.3	33.2±5.6	33.4±6.1	40.8±5.5	36.8±5.2
δ ¹⁵ N ^{SP} _{N2O}	NA	9.4 ±4.5	11.6±5.4	6.9±5.2	9.0±6.2	8.6±3.1
a ¹⁵ N _{N2O} [atom %]	¹⁵ N	7.5 ±2.7	11.7±7.3	16.2±10.6	11.8±0.72	13.7±0.67
f _{P N2O}	¹⁵ N	0.28 ±0.12	0.23±0.13	0.59±0.19	0.69±0.06	0.96±0.09
a _{P N2O}	¹⁵ N	0.28 ±0.07	0.47±0.09	0.26±0.11	0.17±0.02	0.15±0.01
a _{P N2}	¹⁵ N	nd	0.23±0.11	0.33±0.11	0.21±0.07	0.18±0.06

^a determined in ¹⁵N treatments with gas-flux method

^b half of data below detection limit

bd – below detection limit

nd – not determined – due to N₂ flux below detection limit

1220 **Table 3: Comparison of N₂O residual fraction (r_{N_2O}) determined with the N₂O isotopocule approaches (SP/O Map and 3DI model) and the reference method (¹⁵N gas-flux). Minimal (min), maximal (max) and mean values were calculated with the each sampling mean values (of all replicates). The agreement with the reference method was assessed with the Nash–Sutcliffe efficiency (F , Eq. 19) (Nash and Sutcliffe, 1970), which represent the R^2 of the fit to the 1:1 line (Fig. 6).**

		N ₂ O isotopocule approaches				reference method
		SP/O Map		3DI model		¹⁵ N gas-flux
		Case1	Case2	Case1	Case2	
L1	min	0.15	0.14	0.41	0.16	0.03
	max	0.24	0.24	0.71	0.32	0.30
	mean	0.19	0.18	0.49	0.21	0.12
L2	min	0.16	0.15	0.40	0.17	0.12
	max	0.52	0.53	0.71	0.68	0.93
	mean	0.27	0.27	0.49	0.36	0.50
F1	min	0.68	0.70	0.89	0.87	0.75 ^a
	max	1.00	1.00	0.93	0.93	1 ^a
	mean	0.86	0.86	0.91	0.89	nd^a
F2	min	0.30	0.36	0.46	0.22	0.02 ^b
	max	0.43	0.49	0.72	0.61	0.11 ^b
	mean	0.38	0.42	0.58	0.39	0.06^b
F3	min	0.26	0.27	0.39	0.27	0.17
	max	0.47	0.47	0.82	0.42	0.59
	mean	0.33	0.32	0.54	0.34	0.33
agreement with reference method (F)		0.59* $p=0.091$	0.61* $p=0.081$	-0.09	0.77** $p=0.015$	

^a all N₂ fluxes under detection limit, the range of values estimated based on detection limit – values not included in the statistics

^b data not complete due to half of N₂ fluxes under detection limit – values not included in the statistics

1230

Table 4: Comparison of N₂O fraction originating from bD (f_{bD}) determined with the N₂O isotopocule approaches (SP/O Map and 3DI model) and the reference method (¹⁵N gas-flux). Due to methodical assumptions for the particular approach either bD+nD fraction (for SP/O map and 3DI model) or bD+fD fraction (for 3DI model and reference method) can be compared (see Section 3.10).

		N ₂ O isotopocule approaches						reference method
		SP/O Map (bD+nD)		3DI model (bD+nD)		3DI model (bD+fD)		¹⁵ N gas-flux (bD+fD)
		Case1	Case2	Case1	Case2	Case1	Case2	
L1	min	0.96	0.79	0.86	0.84	0.35	0.34	0.64
	max	1	1	0.94	0.94	0.71	0.71	0.75
	mean	0.99	0.93	0.89	0.89	0.59	0.59	0.70
L2	min	0.94	0.88	0.65	0.66	0.65	0.65	0.81
	max	1	1	0.95	0.95	0.97	0.97	1
	mean	0.98	0.96	0.84	0.84	0.82	0.82	0.95
F1	min	0.62	0.55	0.52	0.52	0.85	0.85	0.08
	max	0.84	0.83	0.82	0.82	0.97	0.97	0.42
	mean	0.74	0.70	0.70	0.70	0.91	0.91	0.28
F2	min	0.84	0.64	0.62	0.59	0.34	0.14	0.16
	max	0.95	0.89	0.83	0.83	0.94	0.95	0.31
	mean	0.92	0.77	0.75	0.74	0.65	0.59	0.23
F3	min	0.97	0.92	0.87	0.86	0.21	0.06	0.41
	max	1	1	0.93	0.93	0.92	0.92	0.83
	mean	0.99	0.97	0.90	0.90	0.60	0.56	0.59

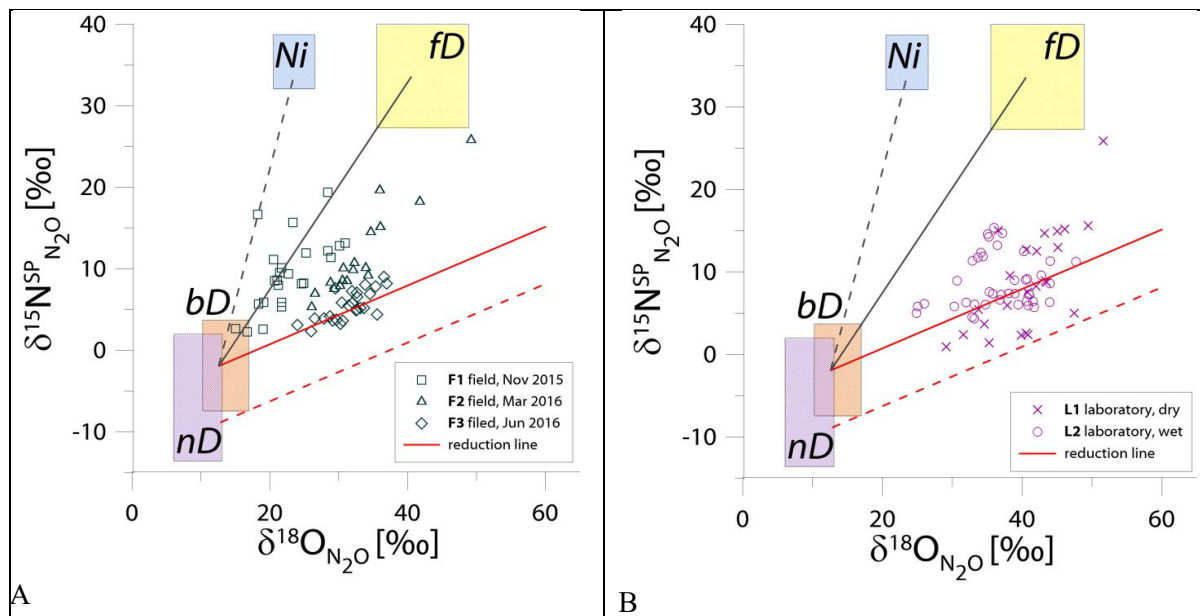


Figure 1: N₂O isotope data of field (A, green points) and laboratory studies (B, purple points) in SP/O Map presented with literature endmember values and theoretical mixing (grey line) and reduction (red line) lines. The solid lines (bD-fD mixing and mean reduction line) are main assumptions used in the calculation procedures for SP/O Map. The grey dashed line shows the alternative bD-Ni mixing line (calculations with this alternative scenario are also presented in the supplement Table S1). The red dashed line shows the minimum reduction line – for the case of minimal delta values of the bD endmember. $\delta^{18}\text{O}$ values of mixing endmembers bD, nD and fD are presented in relation to the mean measured ambient water of -6.4‰ (hence present the expected $\delta^{18}\text{O}_{\text{N}_2\text{O}}$ originating from particular pathway in this study conditions).

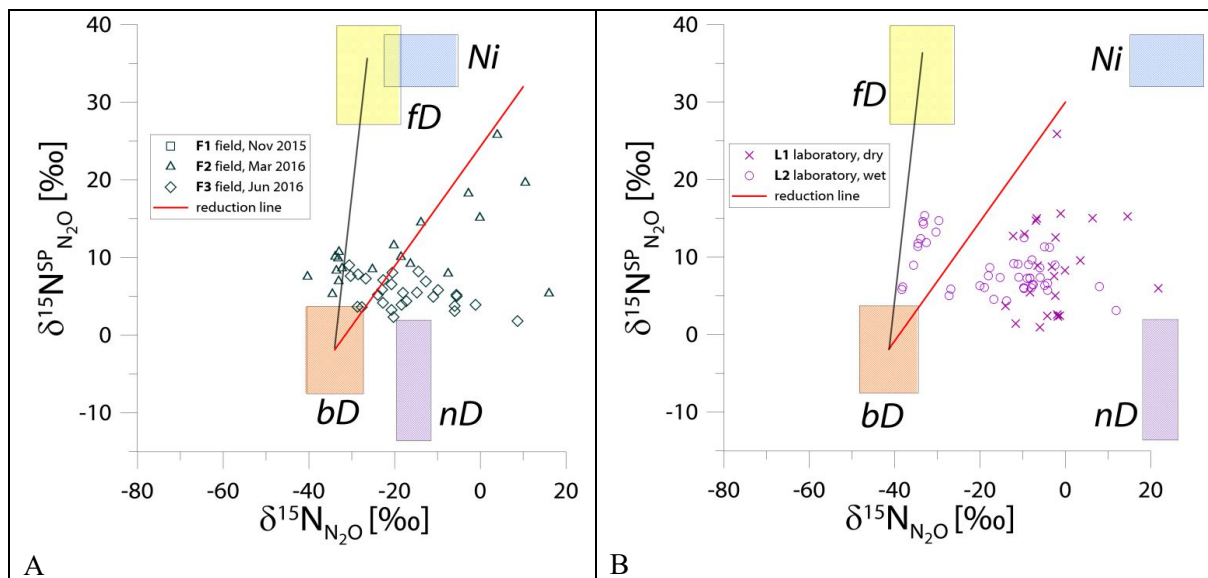


Figure 2: N₂O isotope data of field (green points) and laboratory (purple points) in SP/N Map presented with literature mixing endmember values and theoretical mixing (grey line) and reduction (red line) line. $\delta^{15}\text{N}$ values of mixing endmembers are presented in relation to the $\delta^{15}\text{N}$ of precursors: soil nitrate for bD and fD or ammonium for nD and Ni (hence present the expected $\delta^{15}\text{N}_{\text{N}_2\text{O}}$ originating from particular pathway in this study conditions).

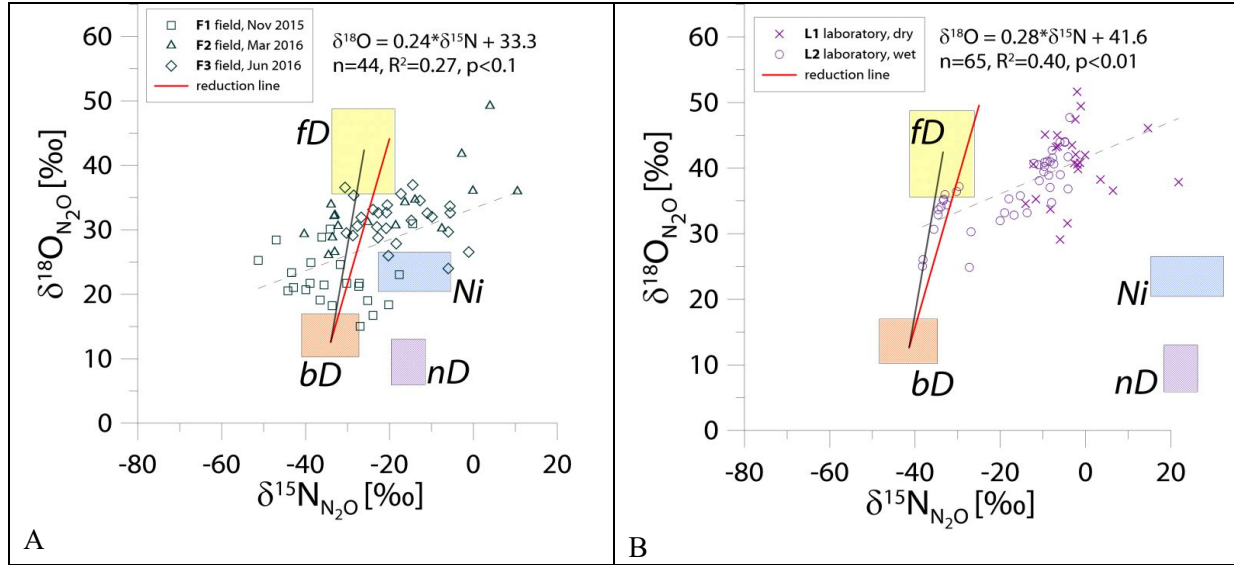


Figure 3: N₂O isotope data of field (A, green points) and laboratory (B, purple points) in O/N Map presented with literature mixing endmember values and theoretical mixing (grey line) and reduction (red line) lines. $\delta^{15}\text{N}$ values are presented in relation to the $\delta^{15}\text{N}$ of precursors: soil nitrate for bD and fD or ammonium for nD and Ni. $\delta^{18}\text{O}$ values of mixing endmembers bD, nD and fD are presented in relation to the mean measured ambient water of -6.4‰. Hence, the mixing endmember ranges present the expected $\delta^{15}\text{N}_{\text{N}_2\text{O}}$ and $\delta^{18}\text{O}_{\text{N}_2\text{O}}$ originating from particular pathway in this study conditions. The dashed line shows the linear fit for all the points with its equation and statistics above.

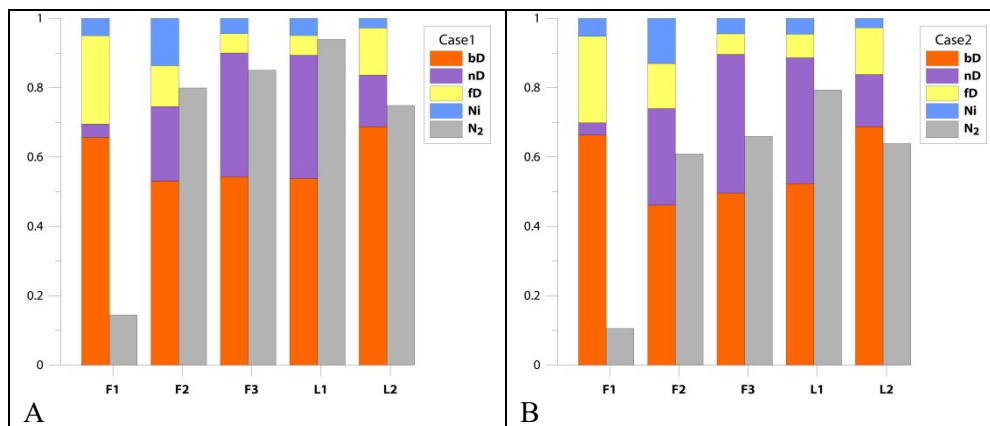


Figure 4: Bar plots showing modeled pathway fractions (f_{bD} , f_{nD} , f_{fD} , f_{Ni}) and N_2 flux contribution in the total (N_2+N_2O) flux $(1-r_{N_2O})$. Results for both modeling cases: Case 1 (A) and Case 2 (B) are shown.

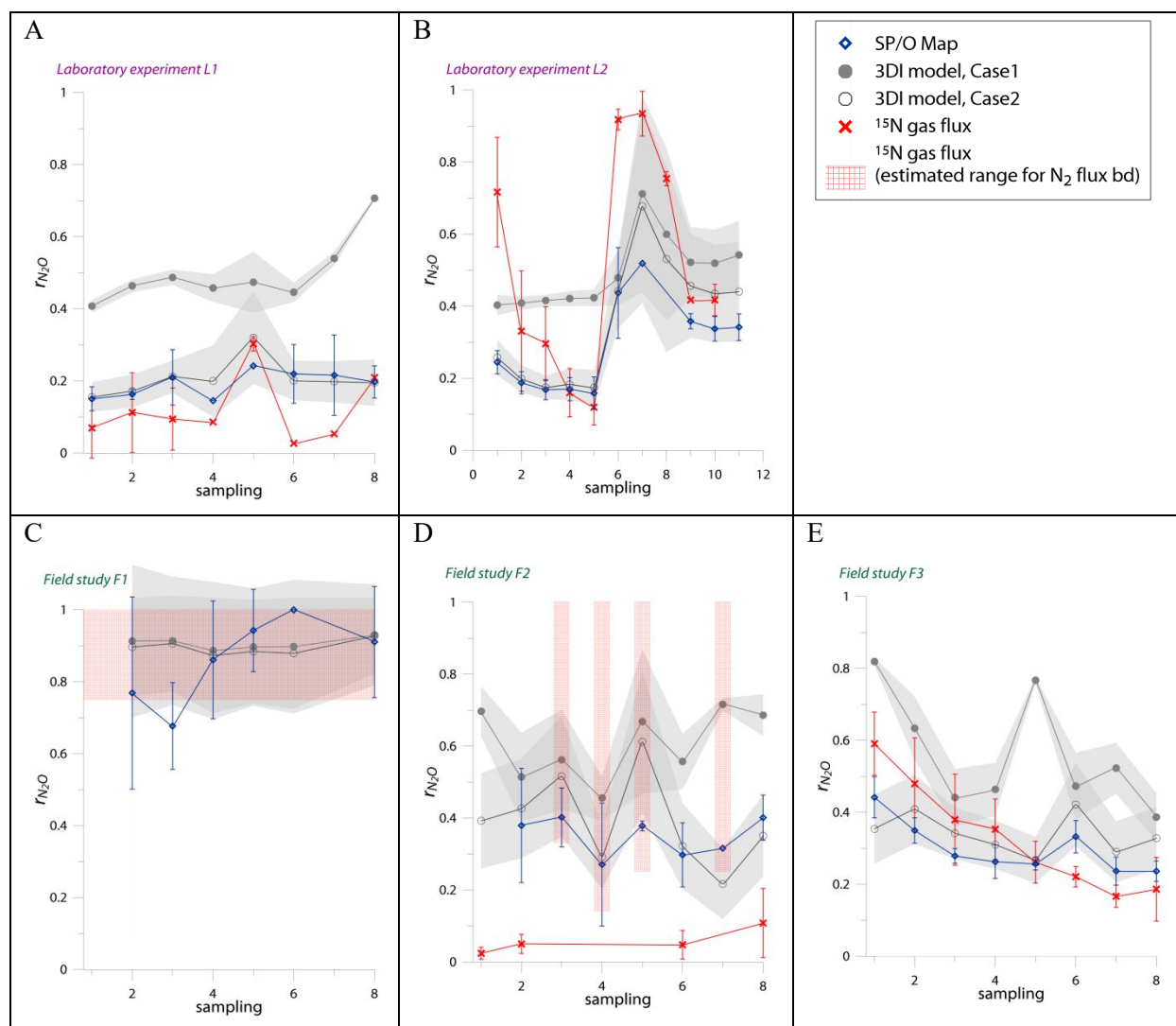


Figure 5: Comparison of time changes in residual N_2O fraction (r_{N_2O}) determined with O/SP Map Case 1 and 3DI model with the reference method (^{15}N gas-flux). For the 3DI model results the 95% confidence interval is shown with grey shaded areas. Error bars for O/SP Map and ^{15}N gas-flux data represent the standard deviation of replicate samples ($n=4$). For N_2 fluxes below the detection limit the estimated r_{N_2O} values are shown (red areas), calculated with N_2 flux from 0 to 1 of the detection limit.

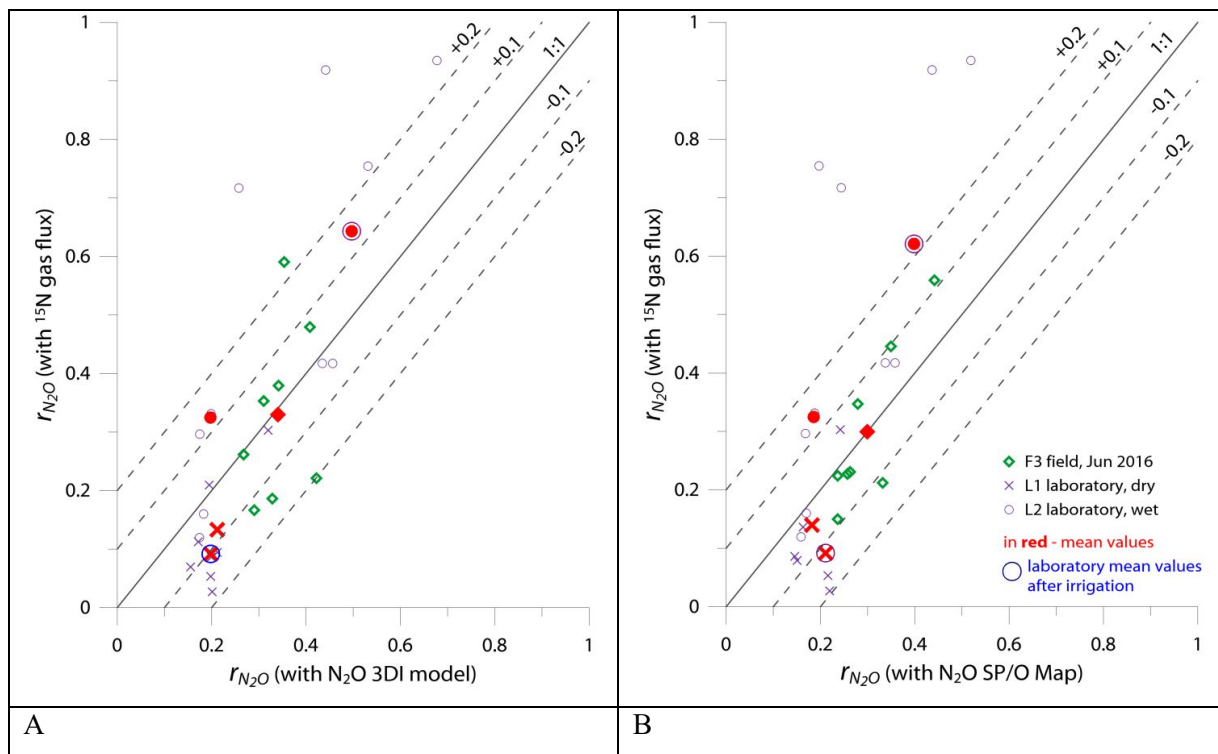


Figure 6: Comparison of 1:1 fit between r_{N_2O} determined with the reference method (^{15}N gas-flux) and (A) 3DI model Case 2, (B) SP/O Map Case 1.

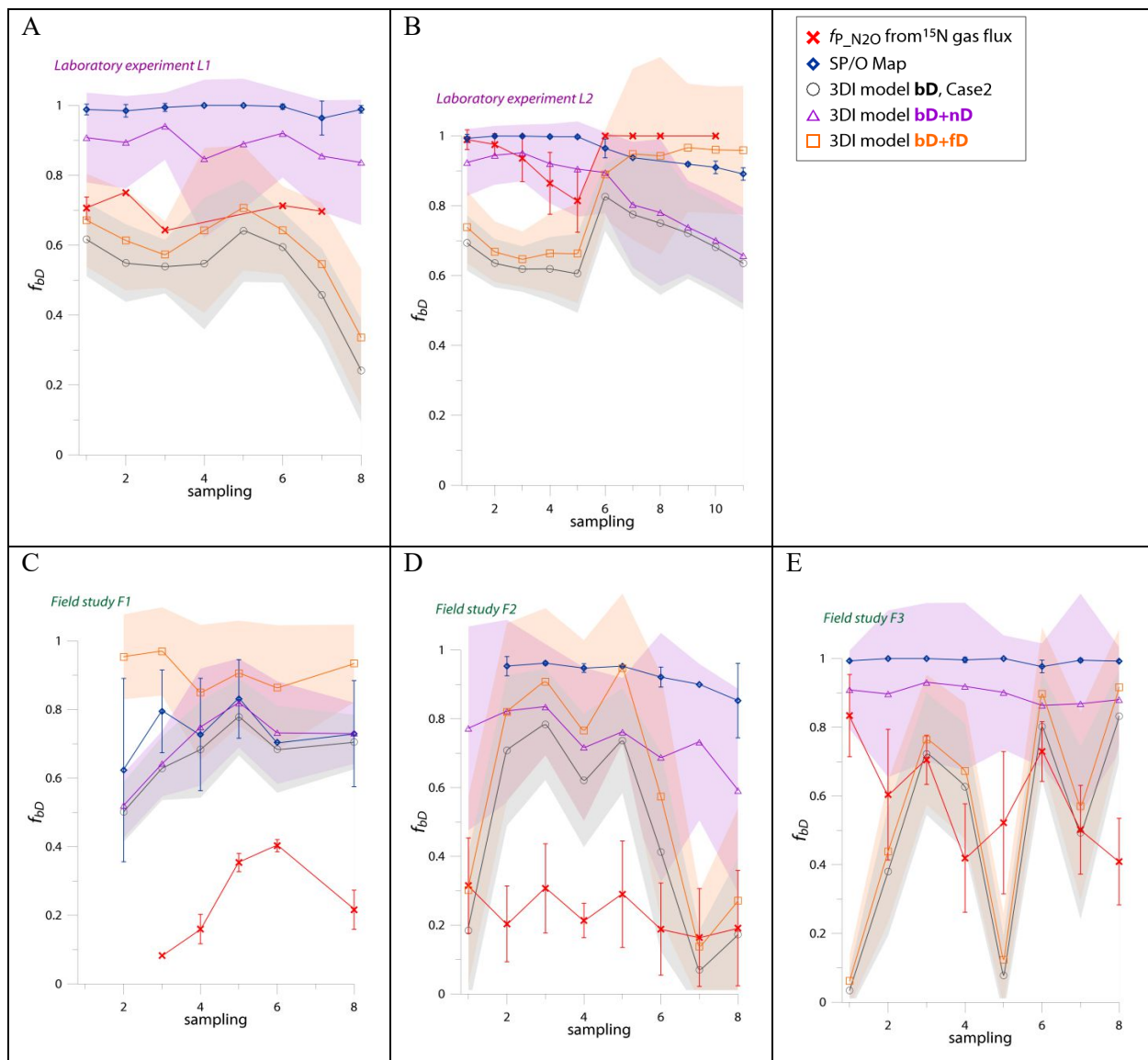


Figure 7: Comparison of N_2O fractions comprising bacterial denitrification (f_{bD}) determined with O/SP Map Case 1 (representing bD+nD) and 3DI model Case 2 (representative fractions determined: bD, bD+nD, bD+fD) with the reference method (^{15}N gas-flux). ^{15}N gas-flux method determines the f_{p_N2O} – ^{15}N -pool derived fraction – comprising all N_2O origins utilizing ^{15}N -labelled NO_3^- – theoretically mostly bD and fD. See Sections 4.2 and 4.3 for further discussion. For the 3DI model results the 95% confidence interval is shown with shaded areas. Error bars for O/SP Map and ^{15}N gas-flux data represent the standard deviation of replicate samples ($n=4$).